

ESA Climate Change Initiative (CCI)

Essential Climate Variable (ECV), Antarctic Ice Sheet (AIS)

Product Validation and Intercomparison Report (PVIR)

Prime & Science Lead: Andrew Shepherd
University of Leeds, UK
A.Shepherd@leeds.ac.uk

Technical Officer: Marcus Engdahl
ESA ESRIN, Frascati, Italy
Marus.engdahl@esa.int

Consortium:

- British Antarctic Survey (BAS)
- Deutsches Zentrum für Luft- und Raumfahrt, Institut für Methodik der Fernerkundung (DLR-IMF)
- DTU-Space, Department of Geodynamics (DTU-GDK)
- DTU-Space, Department of Microwaves and Remote Sensing (DTU-MRS)
- ENVironmental Earth Observation IT GmbH (ENVEO)
- Science [&] Technology AS (S[&]T)
- Technische Universität Dresden (TUDr)
- Technische Universität München (TUM)
- University College London (UCL)
- University of Leeds, Centre for Polar Observation and Modelling (CPOM), (UL)



To be cited as:

M. Horwath, et al., Product Validation and Intercomparison Report (PVIR) for the Antarctic_Ice_Sheet_cci project of ESA's Climate Change Initiative, version 1.3, 04 May 2018.

Available from: <http://www.esa-icesheets-antarctica-cci.org/>

Signatures page



Prepared by	Martin Horwath, Andreas Groh Lead Authors, TUDr	Date: 2018-03-09
Issued by	Kenneth Hauglund Project Manager, S[&]T 	Date: 2018-05-04
Checked by	Andrew Shepherd Science Leader, UL 	Date: 2018-05-04
Approved by	Marcus Engdahl Technical Officer, ESA	

Table of Contents

Change Log	5
Acronyms and Abbreviations	7
1 Introduction	9
1.1 Purpose and Scope	9
1.2 Document Structure	9
1.3 Applicable and Reference Documents	10
2 Surface Elevation Change (SEC)	11
2.1 Independent validation data	11
Requirements	11
Sources	11
Assessment	11
Selection	11
2.2 Validation procedure	12
2.3 Validation outcome	13
2.4 Acknowledgement of the data contributor for SEC validation	17
3 Ice Velocity (IV)	18
3.1 Independent validation data	18
Requirements	18
Sources	18
3.2 Validation procedure	21
3.3 Validation outcome	22
4 Grounding Line Location (GLL)	28
4.1 Independent validation data	28
Requirements	28
Sources	28
Assessment	30
Selection	31
4.2 Validation procedure	31
4.3 Validation outcome	38
Schirmacher area	40
Brunt/Caird	41
PIG 41	
TAM 42	
Identical SAR datasets: MEaSUREs vs. AIS_cci	42
Interpretation and explanation of validation outcome	46
4.4 Recommendations for product improvement	46
4.5 Acknowledgements of data contributors for GLL validation	46
5 Gravimetric Mass Balance (GMB)	47
5.1 Independent validation data	47
Requirements	47
Sources	48
Assessment	48
Selection	49

5.2	Validation procedure.....	49
5.3	Validation outcome.....	50
5.4	Recommendations for product improvement.....	55
5.5	Acknowledgements of data contributors for GMB validation	55
6	References	56

Change Log

Issue	Author	Affected Section	Reason	Status
1.0	M. Horwath, A. Groh Lead Authors, TUDr	All	Document creation	Released to ESA on 2016-04-26
1.1	M. Horwath, A. Groh Lead Authors, TUDr	4	Review input from ESA; Added validation outcome interpretation descriptions for GLL, incl. added §4.3.5	Released to ESA on 2016-05-23
1.2	M. Horwath, A. Groh Lead Authors, TUDr	1, 2.1-2.4, 3.3, 4.3, 4.4, 4.5, 5, 5.3, 5.4, 6	Update for Year 2; SEC: validation extended to ENVISAT period IV: added validation using the latest MEaSURES dataset; GLL: added validation using identical SAR datasets, new paragraph added prior to §4.3.5. Edited recommendation text on 4.4 and updated and added references on 4.5; GMB: updated intro and validation to the latest CRDP, SMB model updated. Updated recommendations References: Updated	Released to ESA on 2017-08-02
1.3	M. Horwath, A. Groh Lead Authors, TUDr	3, 3.2, 3.3 4.3, 4.4 5.1-5.4 6	Update for Year 3: IV: Updated fig 3.1, Added intercomparison of TSX and S1 derived IV maps in the Antarctic Peninsula (+figs); Updated stable rock test results with newly released rock outlines (+ new reference); minor textual changes and corrections; GLL: figures showing the validation outcome updated, text revised GMB: validation based on the latest CRDP; validation data sets updated (SMB, SEC); all figures updated References updated	Released to ESA on 2018-05-04

Distribution List

Organization	Consortium Member
DLR	Dana Floricioiu
DLR	Tanvir Ahmed Chowdhury
DTU - GDK	Rene Forsberg
DTU - MRS	Jørgen Dall
DTU - MRS	Anders Kusk
ENVEO	Thomas Nagler
ENVEO	Jan Wuite
ESA	Marcus Engdahl
S[&]T	Dag Evensberget
S[&]T	Kenneth Hauglund
TUDr	Martin Horwath
TUDr	Andreas Groh
TUM	Alexander Horvath
UCL	Alan Muir
UCL	Steven Baker
UL	Andrew Shepherd
UL	Anna Hogg

Acronyms and Abbreviations

Acronym	Explanation
AIS	Antarctic Ice Sheet
AIS_cci	Antarctic Ice Sheet CCI project
AP	Antarctic Peninsula
APMB	Antarctic Peninsula Mass Balance
AWI	Alfred Wegener Institute for Polar and Marine Research
BAS	British Antarctic Survey
CCI	Climate Change Initiative
CEOS	Committee on Earth Observation Satellites
CF	Climate and Forecasting
CFL	Calving Front Location
CMUG	Climate Modelling User Group
CRG	Climate Research Group
CSR	Center for Space Research
DARD	Dataset Access and Requirements Document
DInSAR	Differential Interferometry
DLR IMF	Deutsches Zentrum für Luft- und Raumfahrt (DLR) Remote Sensing Technology Institute (IMF)
DTU-GDK	DTU Geodynamics Group
DTU-MRS	DTU Microwaves and Remote Sensing Group
EAIS	East Antarctic Ice Sheet
ECMWF	European Centre for Medium-Range Weather Forecasts
ECV	Essential Climate Variable
EGU	European Geophysical Union
ENVEO	ENVironmental Earth Observation GmbH
EO	Earth Observation
ERS	European Remote Sensing Satellite
ESA	European Space Agency
GIS	Greenland Ice Sheet
GCOS	Global Climate Observing System
GLIT	Grounding Line Ice Thickness
GLL	Grounding Line Location
GOS	Global Observing System
GRACE	Gravity Recovery and Climate Experiment
GrIS	Greenland Ice Sheet
IAPG	Institut für Astronomische und Physikalische Geodäsie
ICR	Iceberg Calving Rate
ICSU	International Council for Science
IGOS	Integrated Global Observing Strategy
IMBIE	Ice sheet Mass Balance Intercomparison Exercise
IMF	Ice Mass Flux
InSAR	Interferometry
ICSU	International Council for Science

IOC	Intergovernmental Oceanographic Committee
IOM	Input-Output Method
IPCC	Intergovernmental Panel on Climate Change
IS	Ice Sheets
ITSG	Institute of Theoretical Geodesy and Satellite Geodesy
IV	Ice Velocity
MB	Mass Balance
NASA	National Aeronautics and Space Administration
NERC	Natural Environment Research Council
NetCDF	Network Common Data Form
NSIDC	National Snow and Ice Data Center
PSD	Product Specification Document
RA	Radar Altimetry
SAR	Synthetic Aperture Radar
SEC	Surface Elevation Change
SM	Surface Melt
SMB	Surface Mass Balance
SOW	Statement Of Work
SRD	Systems Requirements Document
STSE	Support to Science Element
S[&]T	Science and Technology AS
TUDr	Technische Universität Dresden
TUM	Technische Universität München
UCL	University College London
UL	University of Leeds
UNEP	United Nations Environment Programme
UNESCO	United Nations Educational Scientific and Cultural Organization
UNFCCC	United Nations Framework Convention on Climate Change
URD	User Requirement Document
URq	User Requirement
WAIS	West Antarctic Ice Sheet
WMO	World Meteorological Organization

1 Introduction

1.1 Purpose and Scope

This document, the Product Validation and Inter-comparison Report (PVIR), is delivered as part of Task 4 of the Antarctic_Ice_Sheet_cci (AIS_cci) project, which is included in Phase 2 of the ESA CCI Program.

The AIS_cci science team has assessed the ECV products in the Climate Research Data Package. An intercomparison of the ECV products with products from other missions and other R&D initiatives has been carried out.

The PVIR describes the results of the validation and inter-comparison exercises, and quantifies the accuracy of the derived products against the validation data and comparable alternative satellite-based products generated by international projects.

The Product Validation and Inter-comparison Report gives a complete report of the activities executed to assessment of the quality of the generated ECV products and the results achieved.

1.2 Document Structure

This document comprises four parts describing each of the parameters of the AIS_cci Essential Climate Variable (ECV). Each parameter has its own chapter as seen below:

- Surface Elevation Change (SEC);
- Ice Velocity (IV);
- Grounding Line Location (GLL);
- Gravimetric Mass Balance (GMB).

Each parameter chapter follows a general structure including

- a description of the requirements for an independent validation data set (Sec. x.1.1)
- a description of available sources of validation data including in-situ observations and alternative data sets (e.g. available products, models, etc.) (Sec. x.1.2)
- a detailed assessment of the validation data including a description of errors and biases as well as uncertainties associated to the data (Sec. x.1.3)
- a description of the selection of validation data sets based on the outlined requirements and assessment of available data (Sec. x.1.4)
- a description of the validation procedure performed on the derived ECV products against the selected validation data sets (Sec. x.2)
- a detailed analysis of the uncertainty of the ECV products with reference to the independent validation data (Sec. x.3)
- recommendations for fixing errors and/or improving the overall product quality (Sec. x.4)

In the interest of brevity, references are given to other project documentation when possible.

1.3 Applicable and Reference Documents

Table 1-1: List of Applicable Documents

No	Doc. Id	Doc. Title	Date	Issue/ Revision / Version
AD1	ESA/Contract No. 4000112227/15/I-NB, and its Appendix 1	Phase 2 of the ESA Climate Change Initiative, Antarctic_Ice Sheet_cci	2015.04.14	-
AD2	CCI-PRGM-EOPS-SW-12-0012 Appendix 2 to contract.	Climate Change Initiative – SoW Phase 2	2014.06.11	Issue 1 Revision 3
AD3	CCI-PRGM-EOPS-TN-12-0031	CCI System Requirements	2013.06.13	Version 1
AD4	CCI-PRGM-EOPS-TN-13-0009	Data Standards Requirements for CCI Data Producers	2013.05.24	Version 1.1

Table 1-2: List of Reference Documents

No	Doc. Id	Doc. Title	Date	Issue/ Revision/ Version
RD1	ST-UL-ESA-AISCCI-URD-001	User Requirement Document (URD)		
RD2	ST-UL-ESA-AISCCI-PSD-001	Product Specification Document (PSD)		
RD3	ST-UL-ESA-AISCCI-DARD-001	Data Access and Requirements Document (DARD)		
RD4	ST-UL-ESA-AISCCI-ATBD-001	Algorithm Theoretical Basis Document (ATBD)		
RD5	ST-UL-ESA-AISCCI-ATBD-002_RR	Algorithm Theoretical Basis Document (ATBD), Appendix Round Robin Experiments		
RD6	ST-UL-ESA-AISCCI-CECR-001	Comprehensive Error Characterisation Report (CECR)		
RD7	ST-UL-ESA-AISCCI-SSD-001	System Specification Document (SSD)		
RD8	ST-UL-ESA-AISCCI-SVR-001	System Verification Report (SVR)		
RD9	ST-UL-ESA-AISCCI-PUG-001	Product User Guide (PUG)		
RD10	ST-UL-ESA-AISCCI-PVIR-001	Product Validation and Inter-comparison Report (PVIR)		
RD11	ST-UL-ESA-AISCCI-CRDP-001	Climate Research Data Package (CRDP)		
RD12	ST-UL-ESA-AISCCI-CAR-001	Climate Assessment Report (CAR)		
RD13	ST-UL-ESA-AISCCI-PMP-001	Project Management Plan (PMP)		

Note: If not provided, the reference applies to the latest released Issue/Revision/Version

2 Surface Elevation Change (SEC)

This chapter gives a complete report of the activities carried out to assess the quality of the SEC products.

2.1 Independent validation data

Requirements

The data sets used to validate the Surface Elevation Change (SEC) product must have been acquired in Antarctica, be freely available for the project to use, must overlap either fully or partly with the satellite radar altimetry time series used to produce the SEC product, and must be able to be used to measure surface elevation change.

Sources

Airborne Topographic Mapper (ATM) airborne elevation data has been collected in Antarctica on numerous operation Icebridge campaigns between 1993 and the present day.

Assessment

The airborne validation data sets are produced from data acquired by laser altimeter, therefore it is anticipated that there may be some bias in the validation results because the laser altimeters reflect off the ice surface, whereas the satellite radar altimeters penetrate some depth into the snowpack.

ASIRAS is an airborne radar altimetry instrument that operates at 13.5GHz, the same central frequency as CryoSat-2. This dataset is likely to be subject to similar penetration effects as the satellite radar altimetry data used to produce the SEC product. Recently the ATM level 4 SEC product has been released, allowing direct comparison of surface elevation change between separate instruments.

It should be noted that the CCI SEC product is calculated over the Envisat mission period and the CryoSat-2 mission period to end 2016, whereas the ASIRAS dataset is acquired during various shorter periods within the limits of the CCI SEC product time periods.

Selection

All available validation data acquired in Antarctica was used to validate the Antarctic CCI SEC product. The data sets used were acquired from 2002 onwards to coincide with the Envisat and CryoSat-2 missions. In future years once the full 25 year time series has been compiled we will perform a full validation on the whole satellite radar altimetry dataset.

Airborne data locations used to validate AIS CCI SEC

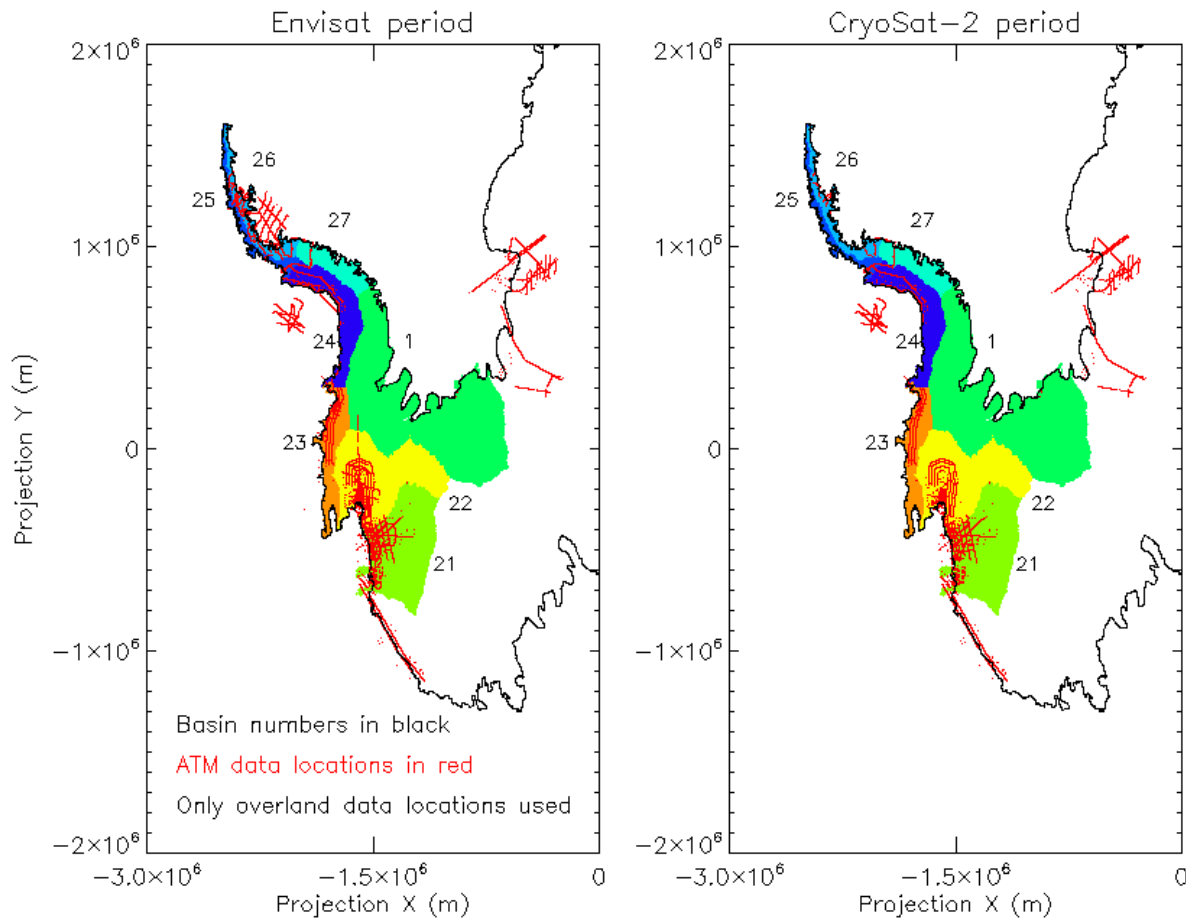


Figure 2.1: Map showing the geographic distribution of the airborne datasets used to validate the Antarctic cci surface elevation change product. Map projection is polar stereographic based on WGS84, central longitude 0E, central latitude 71S. Drainage basins are based on the Zwally definitions.

2.2 Validation procedure

Surface elevation change trends from all available airborne validation datasets within the marked basins (ie basin 1 and basins 21 to 27) were compared against the surface elevation change trends measured from the long time series of satellite radar altimetry surface elevation change data from Antarctica. The airborne data outside the marked basins could not be properly compared to Envisat data as it is south of Envisat's latitude limit.

Since the CCI SEC product is calculated from modelling based on 5km by 5km cells, the ASIRAS product was averaged over each cell, using a resistant mean (ie, excluding outlying datapoints more than 3 standard deviations from the mean of the entire cell dataset) before comparison. The difference was calculated as ASIRAS minus CCI SEC.

The terrain in each drainage basin varies. The CCI SEC product is expected to perform at its best over ice sheets, ie regions of low slope. However, the available comparison data covered many terrains. Consequently separate results for each drainage basin are given, and the mean slope of each basin is tabulated.

2.3 Validation outcome

The CCI SEC product was determined for the region of interest, shown in Figure 2.2, below.

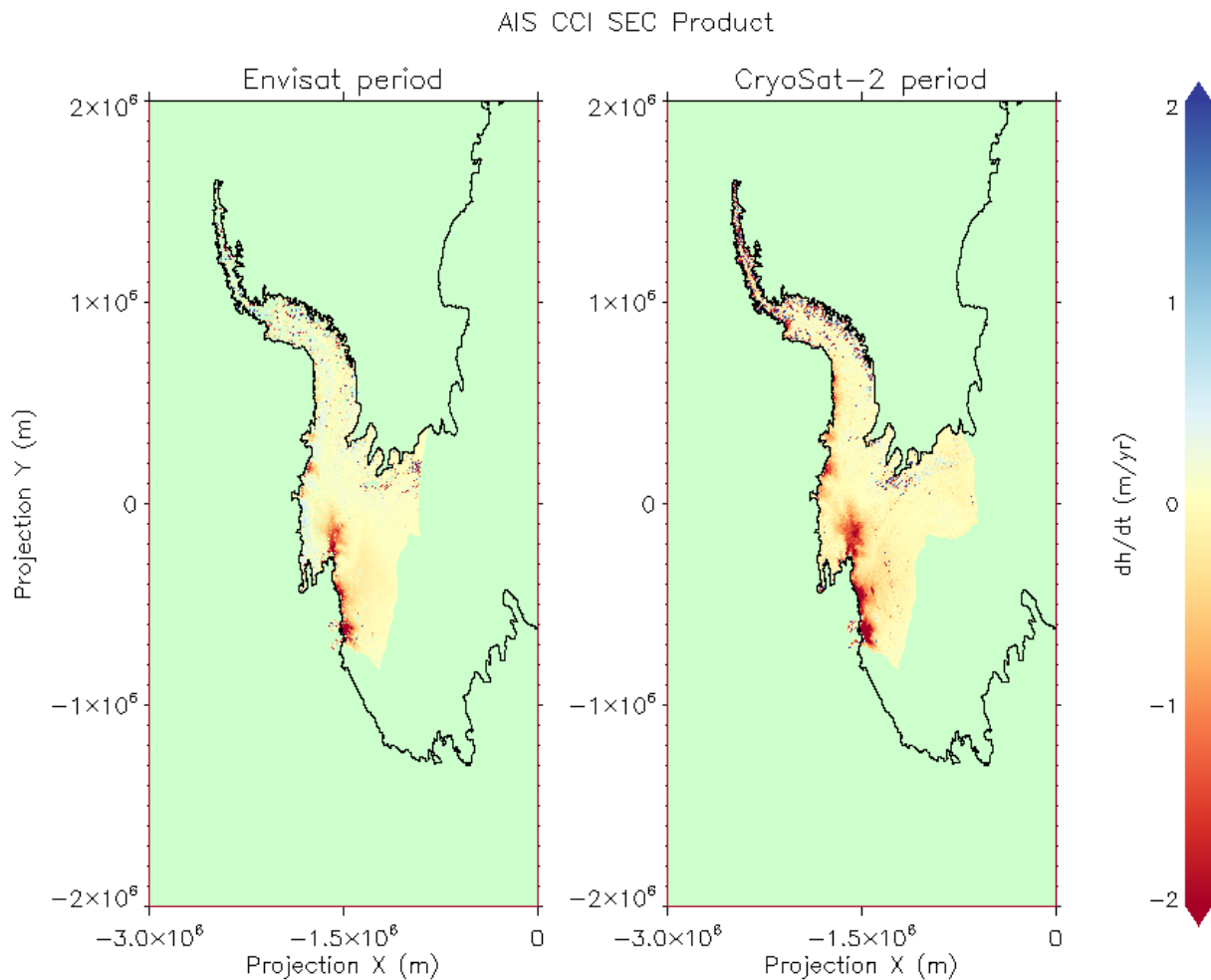
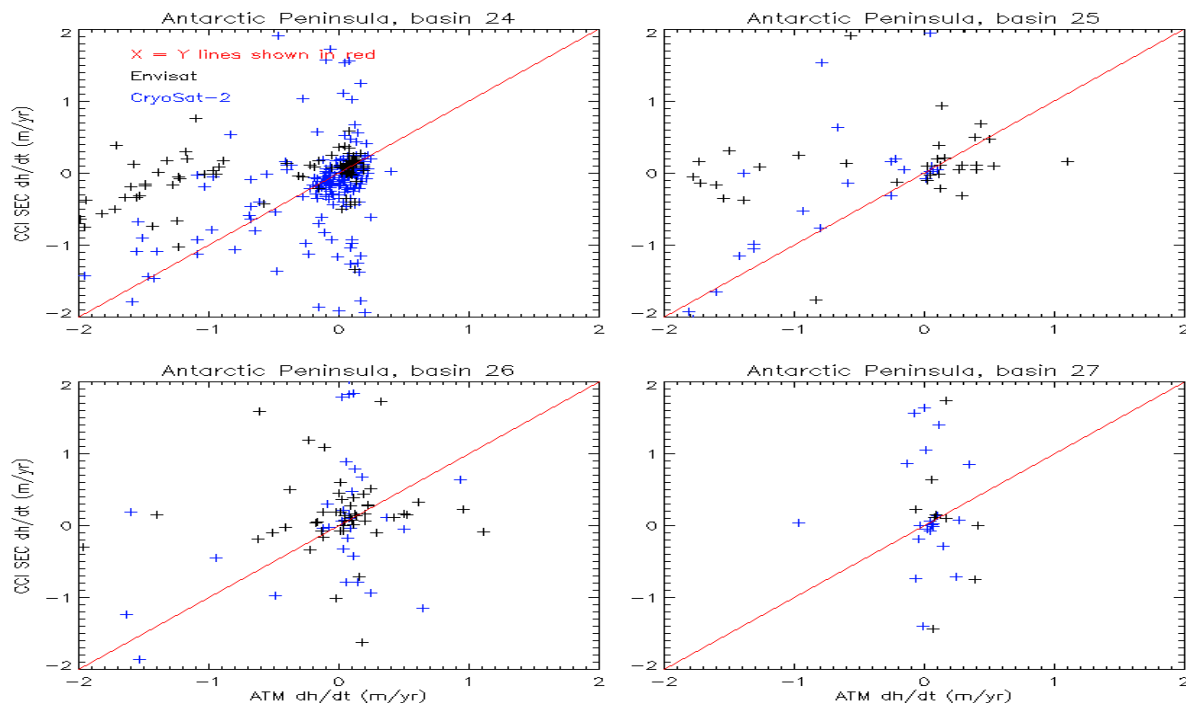


Figure 2.2: Two maps showing the surface elevation change measured in the validation region, over the Envisat and CryoSat-2 mission periods. Projection as for Figure 2.1. The Antarctic Peninsula consists of basins 24 to 27. Basins 1 and 21 to 23 are in the West Antarctic.

The results of the comparison with the averaged-by-cell airborne data are shown as scatter plots below. These have been split into basins in the Antarctic Peninsula and West Antarctic regions.

a)



b)

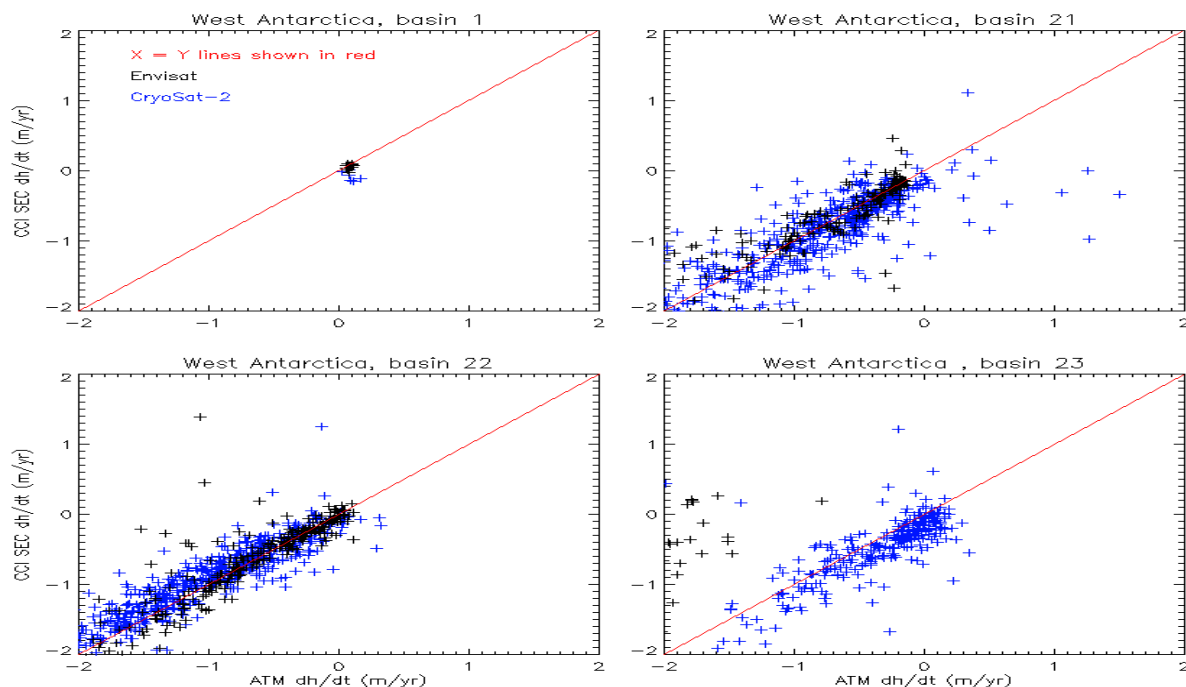
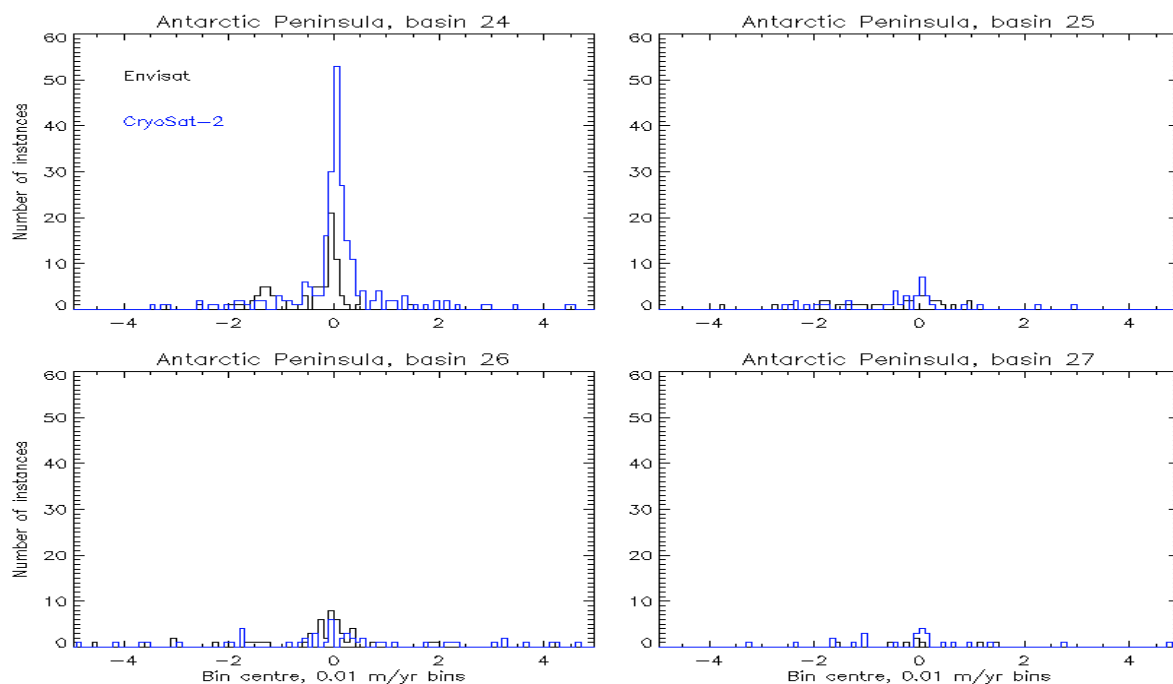


Figure 2.3: Two sets of scatter plots showing the difference between the satellite surface elevation change from the CCI SEC product, and the airborne surface elevation change. These split the regions of interest into basins in a) the Antarctic Peninsula, b) West Antarctica. Black datapoints are from the comparison to Envisat, blue to CryoSat-2.

Histograms of the results, showing the distribution of the difference between the two products, are given below.

a)



b)

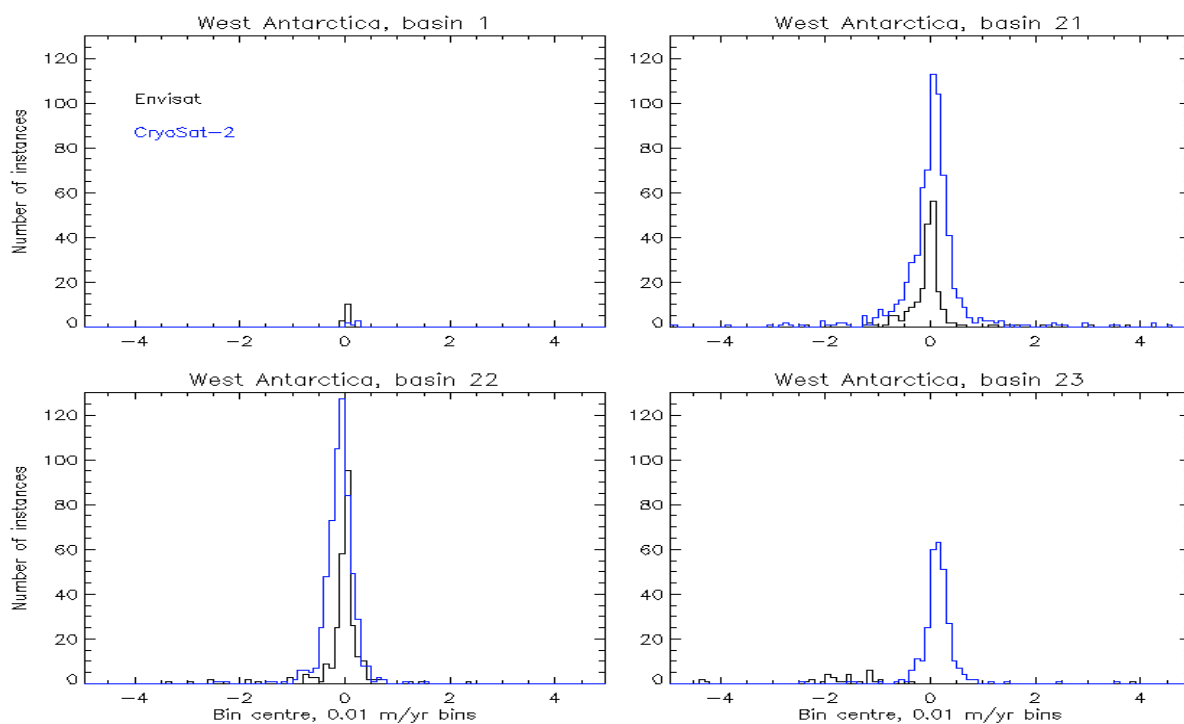


Figure 2.4: Two sets of histograms showing the bias between the satellite surface elevation change from the CCI SEC product, and the airborne surface elevation change. These split the region of interest into basins in a) the Antarctic Peninsula, b) West Antarctica. Black datapoints are from the Envisat period, blue from CryoSat-2. Note that the Y axes are not the same on all plots, to make the contents more visible.

Statistics on the difference in change, ASIRAS minus CCI SEC, for each basin are tabulated below. The number of cells used in each basin is noted as the SEC products were only compared when a result existed for both datasets. Comparison statistics are calculated from a restricted dataset which excludes outliers by only considering data points within ± 3 standard deviations from the mean of the whole, original dataset. The mean slope of the cells used in each basin is also noted, as a measure of its terrain variability.

Table 2-1: Tables, by mission period showing statistics of the difference between the ASIRAS and CCI SEC datasets for all validation basins. Figures rounded to two decimal places.

a) Envisat

	Mean (m/yr)	Minimum (m/yr)	Maximum (m/yr)	Standard deviation (m/yr)	RMS (m/yr)	Number of cells considered	Basin mean slope (degrees)
AP, basin 24	-0.25	-1.26	0.53	0.06	0.53	73	1.75
AP, basin 25	-0.56	-2.78	0.95	0.17	1.13	36	7.37
AP, basin 26	-0.19	-2.00	1.19	0.09	0.67	48	10.57
AP, basin 27	0.06	-1.57	1.50	0.31	0.86	9	1.88
WA, basin 1	0.02	-0.03	0.06	0.01	0.03	13	0.25
WA, basin 21	-0.03	-0.51	0.47	0.01	0.18	175	1.18
WA, basin 22	0.02	-0.38	0.40	0.01	0.14	242	0.72
WA, basin 23	-1.52	-2.33	-0.35	0.09	0.59	30	6.54

b) CryoSat-2

	Mean (m/yr)	Minimum (m/yr)	Maximum (m/yr)	Standard deviation (m/yr)	RMS (m/yr)	Number of cells considered	Basin mean slope (degrees)
AP, basin 24	0.04	-0.60	0.72	0.02	0.24	179	1.28
AP, basin 25	-0.47	-2.37	1.19	0.15	0.99	34	2.10

AP, basin 26	-0.10	-7.26	6.77	0.38	2.70	53	3.89
AP, basin 27	-0.29	-3.27	2.76	0.26	1.25	24	6.76
WA, basin 1	0.17	0.04	0.28	0.04	0.19	6	0.50
WA, basin 21	0.03	-0.78	0.86	0.01	0.28	613	0.61
WA, basin 22	-0.09	-0.68	0.49	0.01	0.22	568	0.49
WA, basin 23	0.14	-0.38	0.63	0.01	0.24	274	0.86

In summary these results show that the mean difference between the validation dataset and the SEC product is less than 1 metre per year in all areas except the poorly sampled and highly sloping basin 23, with the lowest differences generally occurring in West Antarctica. We attribute the larger difference between the validation data and the SEC product on the Antarctic Peninsula, in comparison to West Antarctica, to the more steeply sloping topography which is known to be more challenging terrain for the altimeter data retrieval to operate in.

We will improve the SEC data validation in future years by extending the validation to other areas such as East Antarctica, and extending the validation back in time to the early 1990's, although it is recognised that there are severely limited validation datasets available to perform this task.

2.4 Acknowledgement of the data contributor for SEC validation

The following dataset was used for the present validation:

Studinger, M. S. 2014, updated 2016. IceBridge ATM L4 Surface Elevation rate of Change, Version 1, Antarctica subset. Boulder, Colorado, USA. NASA National Snow and Ice Data Center Distributed Active Archive Centre. Doi:<http://dx.doi.org/10.5067/BCW6CI3TXOCY>. Accessed 25th May 2017.

3 Ice Velocity (IV)

This chapter gives a complete report of activities carried out to assess the quality of the IV products **generated within AIS CCI**. For this purpose we use averaged Antarctica wide IV **maps** derived by offset tracking using Sentinel-1 (S1) data (**versions: v20160217 and v20170428**; Figure 3.1) as well as ice velocity **maps** derived from single S1 image **pairs** covering Pine Island Glacier (PIG) and the **Antarctic Peninsula (API)**. Several QA tests are performed using independent validation data. The results of these tests are described below.

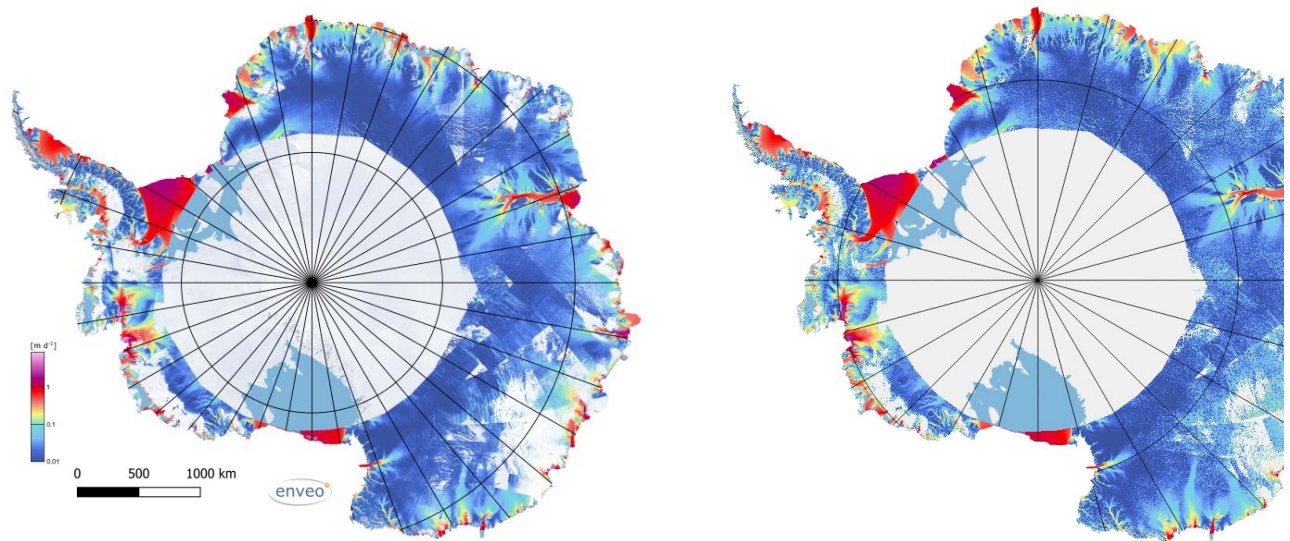


Figure 3.1: Antarctica wide IV map, derived from S1 data acquired in the period, left: Aug 2015-Jan 2016 (v20160217), right: Aug 2015-April 2017 (v20170428).

3.1 Independent validation data

Requirements

The comparison of satellite derived velocity products with in-situ measured velocity data, e.g. GPS, represents the highest level of validation. However, the comparison of space-borne glacier velocity estimates with in-situ data is complicated by several issues. Though highly precise, the temporal and spatial representativeness of the GPS data compared to the area and time covered by the image data to be validated will vary and is not strictly known. **Additionally**, for calculation of statistical parameters the number of in-situ data and corresponding EO observations has to be statistically significant. For Inter-comparison of IV products from different sensors in general the product must be evaluated against a product derived from higher resolution data, providing better quality of IV maps from offset tracking.

Sources

In-situ GPS: In-situ raw GPS positions acquired using javelins are provided by BAS. Javelins are GPS equipped devices launched from a plane at low altitude which record and transmit position at varying time intervals (seconds to hours) while moving along flow. The provided text files include Javelin ID, EPOCH timestamp, Latitude and Longitude. In total 23 javelins were successfully deployed on Pine Island Glacier (PIG), collecting data for various epochs between January 2013 and April 2015. Figure 3.2 shows in different colors the path of the GPS recorders on PIG and a close-up showing

that over short intervals the recorded position can fluctuate significantly (up to 100s of m). **Therefore**, we use positions acquired during the whole operational period to calculate the average ice velocity by fitting a polynomial through all positions and dividing by the total time interval for each GPS recorder. As such the time period by the GPS data is not exactly the same as the period covered by the Sentinel-1 IV map.

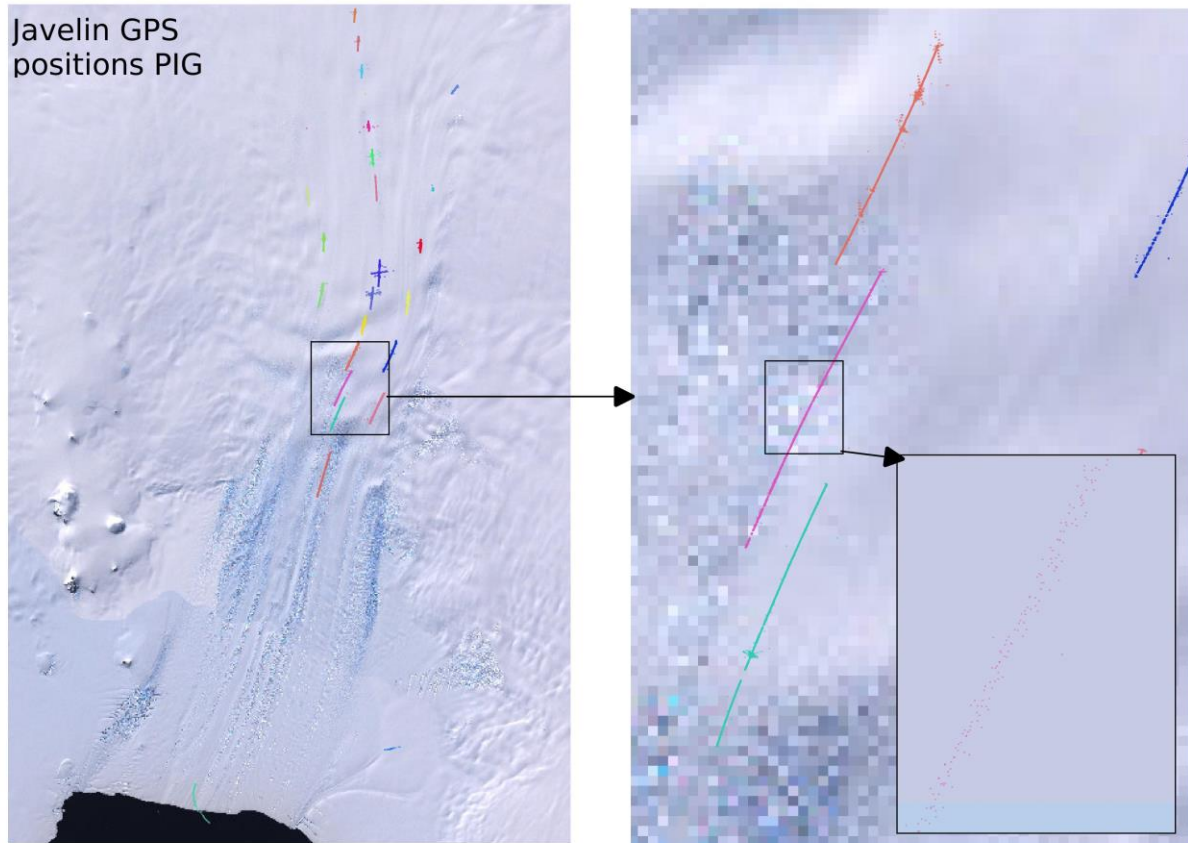


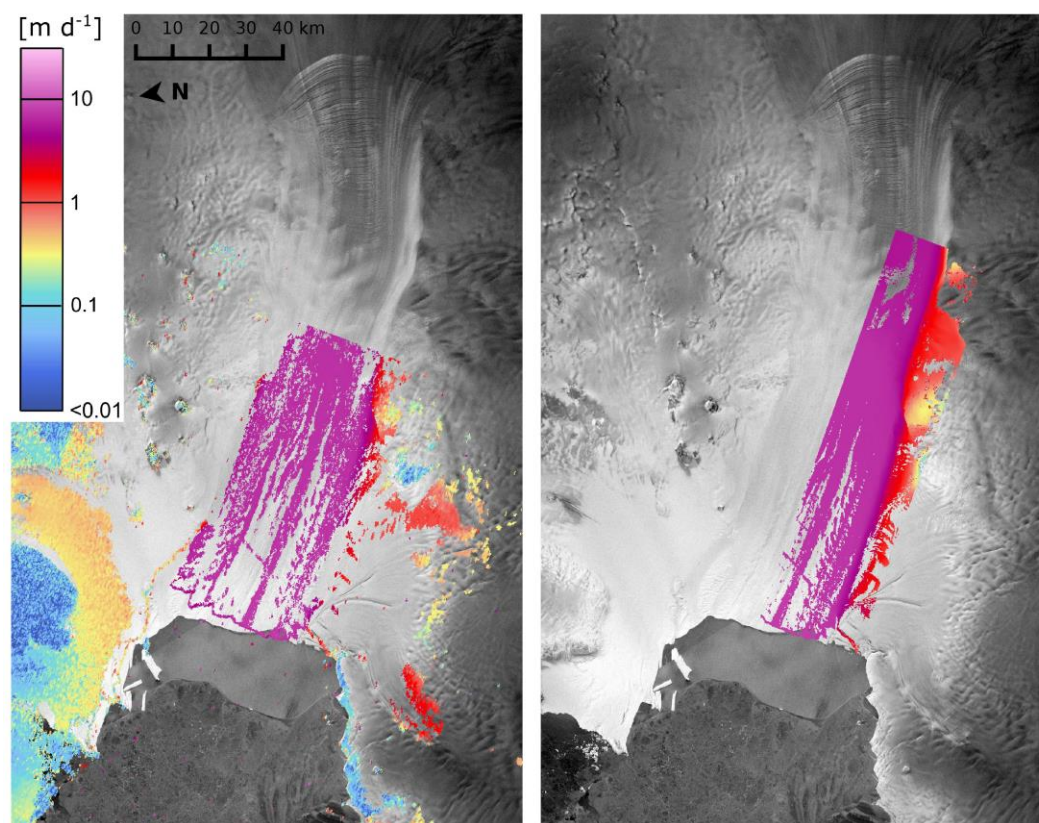
Figure 3.2: Left: Overview of javelin GPS locations and paths; right: Close up of area depicted left. Background LIMA Landsat mosaic (USGS).

TerraSAR-X: For the cross-sensor comparison of the S1 IV time-series of Pine Island Glacier a repeat pass TerraSAR-X (TSX) image pair (period 06.24.2015–07.05.2015), covering a section of the glacier, is selected and used to derive IV. For comparison the S1 IV map closest in time is used (06.19.2015–07.01.2015). Table 3-1 gives a comparison of the satellite and product characteristics of the data sets. Figure 3.3 shows the derived velocity fields using S1 and TSX SAR data.

We extend the intercomparison between S1 and TSX using IV maps generated in the project named SAR Algorithms for Mass Balance and Dynamics of Calving Glaciers (SAMBA). SAMBA is an ESA funded collaboration between ENVEO and DLR and lead by the latter. The main goal is to advance the utilization of high resolution SAR sensors for better understanding of flow dynamics and processes of ice/climate interactions of calving glaciers. One of the key areas of interest for SAMBA is the Antarctic Peninsula (API).

Table 3-1: Overview of satellite and product characteristics.

SAR Platform	Sentinel-1	TSX
Sensor	C -band SAR	X -band SAR
Mode / Product	IWS / SLC	Stripmap / SSC
Swath width	250km	30x50 km
Resolution	3 x 22m	1.2 × 3.3m
Repeat cycle	12d	11d
Track	65	77 (strip 19)
Dates	06/19/15 – 07/01/15	06/24/15 – 07/05/15
Gridsize IV map (m)	200	200


Figure 3.3: Ice velocity on Pine Island Glacier derived using Sentinel-1 (left) and TSX (right).

MEaSURES: As part of the NASA Making Earth System Data Records for Use in Research Environments (MEaSURES) Program a high-resolution digital mosaic of ice motion in Antarctica was assembled derived from multiple satellite interferometric synthetic-aperture radar data acquired during the International Polar Year (2007-2009) (Rignot, 2011). The map combines data derived from 2009 RADARSAT-2, 2007-2009 Envisat (ASAR), 2007-2008 ALOS (PALSAR), 2000 RADARSAT-1 and 1996 ERS-1 and ERS-2. Data are available through NSIDC at 450 m and 900 m spacing, for validation purposes the 450 m product is used. In April 2017 an updated version of the

MEaSURES ice velocity map was released (version 2). The main update to the data set is the inclusion of IV data from 2011-2016 acquired from RADARSAT-2, Sentinel-1, TerraSAR-X, TanDEM-X as well as Landsat-8 optical imagery. In addition, the mosaicking method was adjusted.

3.2 Validation procedure

For quality assessment (QA) of IV products a series of standard test/measures are developed (adopted from ESA Glaciers_CCI) providing various levels of validation. Table 3-2 gives an overview of the QA tests and the metrics that it provides. The tests are described in more detail below.

Table 3-2: Summary of QA tests and the metrics that it provides.

Test	Description	Metrics
QA-IV-1	Intercomparison with in-situ data (e.g. in-situ GPS).	Mean, RMSE [m/day] East/North
QA-IV-2	Sensor cross-comparisons: Inter-comparison of IV products from different sensors.	Mean, RMSE [m/day] East/North
QA-IV-3	Intercomparison of IV products with available existing IV datasets (e.g. MEaSURES, AMM, Velmap)	Mean, RMSE [m/day] East/North
QA-IV-4	Local measure of IV quality estimate, attached to the product; estimates are CC, Number of available values for each pixel, STD	CC, STD
QA-IV-5	Mean and RMSD of the velocity over stable terrain; mean values should be 0.	Mean, RMSE [m/day] East/North

QA-IV-1 Comparison of satellite derived velocity products with in-situ measured velocity data (GPS). The quality metrics of this test provides: Mean and RMSD of the difference in velocity of IV products and in-situ data.

QA-IV-2 Here we apply the comparison of velocity fields generated from independent data sets from different sensors covering roughly the same period. The quality metrics of this test provides: Mean and RMSD of the difference of velocity components (E,N,Z).

QA-IV-3 The product is evaluated against publicly available products covering the same area. These generally cover a different time span and are assembled from different sensors. **Nevertheless**, they provide a level of quality assurance, in particular in areas where little change is to be expected (e.g. inland ice sheet). Here we apply the comparison using the averaged Sentinel-1 Antarctica wide velocity map. The quality metrics of this test provides: Mean and RMSD of the difference of velocity components (E,N).

QA-IV-4 This is an internal QA method. Within the processing chain of the IV product generation local quality measures of the IV retrieval are estimated, like the Cross-Correlation Coefficient (CC) and the number and STD of available values for each pixel. These measures quantify the quality of the local IV estimates and are attached to each product.

QA-IV-5 Another internal QA method widely applied for quality assessment of velocity products is the analysis of stable ground where no velocity is expected. This gives a good overall indication for the bias introduced by the end-to-end velocity retrieval including co-registration of images, velocity retrieval, etc. After performing the

matching for the entire region covered by the image pair, the results for the ice covered (moving) area will be separated from ice-free (stable) ground. The masking will be done using a polygon of the glacier/rock outline. Buffers around the polygons are applied before extraction of stable ground for statistic calculation, or alternatively a final visual check for misclassified stable terrain will be performed in order to avoid potential errors introduced by the area polygon. The quality metrics of this test provides: Mean and RMSD of the velocity over stable terrain; mean values should be close to 0.

3.3 Validation outcome

QA-IV-1 Figure 3.4 (left panel) is a scatter plot in which GPS derived velocities are plotted against co-located velocity grid cells extracted from the averaged Antarctica wide IV map (Figure 3.1). The figure shows a good agreement between the GPS and IV velocity. In Figure 3.4 (right panel) GPS flow vectors (green) are visualized alongside flow vectors derived from Sentinel-1 (black) further confirming the agreement.

Table 3-3 lists the IV values for each of the GPS stations and corresponding Sentinel-1 IV. Differences are generally in the order of up to a few percent (mean $< 5 \text{ cm d}^{-1}$, std $< 10 \text{ cm d}^{-1}$). These can partly be attributed to uncertainties inherent to both methods, different averaging time spans, different time frames, or difference in spatial sampling: GPS measures a point location, while the feature tracking procedure averages an area for which the size is based on the window size used for image correlation.

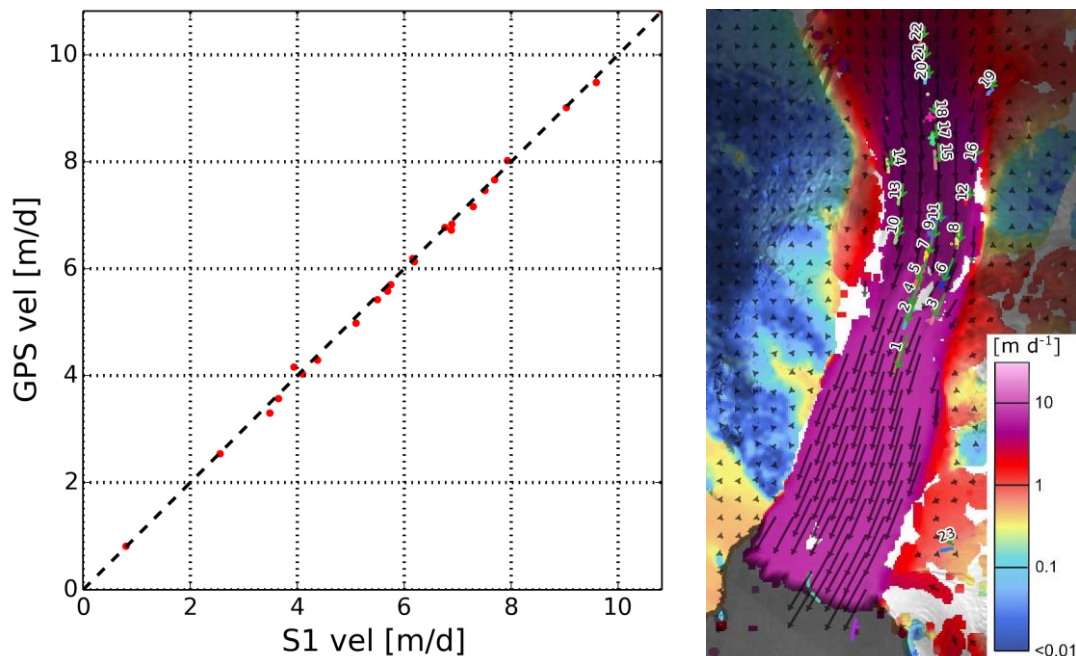


Figure 3.4: Left: Sentinel-1 ice velocity (horizontal magnitude) plotted against GPS velocity, and right: Sentinel-1 derived flow vectors (black) and GPS tracks (green) displayed on the IV map.

Table 3-3: Comparison of in-situ GPS velocity and velocity derived from feature tracking using Sentinel-1. (GPS IDs depicted in Figure 3.4).

GPS ID	GPS (Vh) [m d ⁻¹]	S1 (Vh) [m d ⁻¹]	Difference[m d ⁻¹]
1	10,82	10,82	0,00
2	9,48	9,59	-0,11
3	8,02	7,93	0,09
4	9,01	9,03	-0,02
5	7,46	7,51	-0,05
6	7,66	7,69	-0,03
7	6,72	6,88	-0,16
8	7,16	7,29	-0,13
9	6,77	6,76	0,01
10	5,70	5,75	-0,05
11	6,83	6,89	-0,06
12	6,13	6,19	-0,06
13	5,42	5,50	-0,08
14	4,29	4,38	-0,09
15	6,19	6,16	0,03
16	4,16	3,94	0,22
17	5,58	5,69	-0,11
18	4,98	5,10	-0,12
19	2,54	2,56	-0,02
20	4,03	4,10	-0,07
21	3,57	3,65	-0,08
22	3,30	3,49	-0,19
23	0,81	0,80	0,01
Mean Difference:			-0,047 m d ⁻¹
RMSE:			0,097 m d ⁻¹

QA-IV-2

Pine Island Glacier Here we present difference histograms for the easting, northing and vertical components including statistics. The generated figures and statistics illustrate the performance and level of agreement between the Sentinel-1 and TSX IV datasets. The mean difference is 0.03 m d⁻¹ (RSME: 0.22 m d⁻¹), 0.01 m d⁻¹ (RSME: 0.30 m d⁻¹) and 0.00 m d⁻¹ (RSME: 0.03 m d⁻¹) for the easting, northing and vertical component respectively. This difference can on one hand be explained by the slightly different acquisition period and possibly tidal influences. On the other hand differences near shear zones and margins are related to sensor resolution and window size/settings.

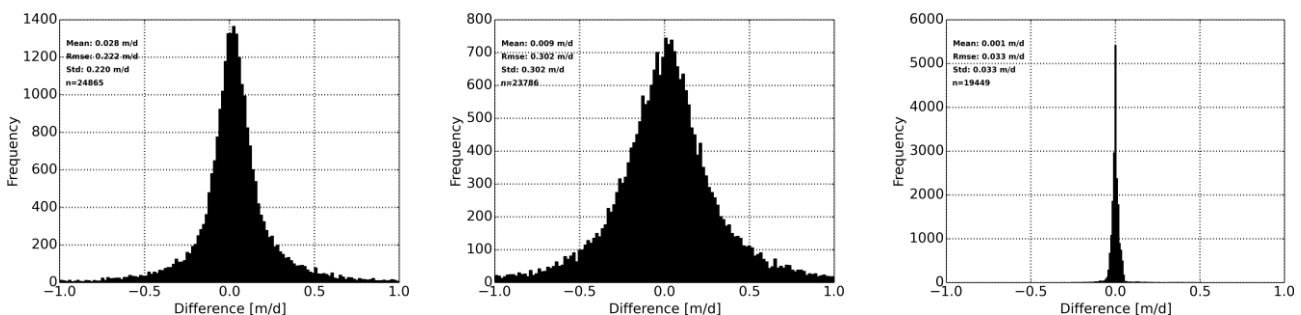


Figure 3.5: QA-IV-2: Difference histograms for easting (left), northing (center) and vertical components (right).

Antarctic Peninsula Only datasets with a maximum time difference of 10 days are used. We inter-compare both the easting and northing components separately on a pixel-by-pixel basis (ignoring the vertical component). As a measure of quality, statistics on the mean, the standard deviation and the root mean square error (RMSE) of the residuals (defined here as Sentinel-1 IV minus TSX IV) are provided. Excluding the IV maps that do not fall within the desired temporal range leaves ~30 usable IV maps. The statistics are summarized in Table 3-4. The overall mean bias between the two data sets is about 1 cm/d for Ve and 0.2 cm/d for Vn with an RMSE of 0.18 m/d and 0.21 m/d for Ve and Vn respectively. Figure 3.6 visualises the comparison and statistical results for the easting (Ve) and northing (Vn) components in a histogram of residuals and a scatterplot. Differences between the data sets can have a variety of causes such as different resolution of SAR data (TSX vs. Sentinel-1), different settings used for IV retrieval (e.g. matching window), differences in post processing (e.g. outlier removal, gap filling) or actual short-term velocity fluctuations. In general, higher resolution satellite data captures velocity better, in particular in shearing zones, where velocity gradients are high.

Table 3-4: Sentinel-1 and TSX ice velocity product intercomparisons for API data sets. Mean, standard deviation (STD), root mean square difference (RMSE) of the residuals (S1 minus TSX) and sample size (n) for both Ve (easting) and Vn (northing) components.

Ve Residual [m/d]				Vn Residual [m/d]			
Mean	STD	RMSE	n [#]	Mean	STD	RMSE	n [#]
0.011	0.175	0.175	572469	-0.002	0.207	0.207	570908

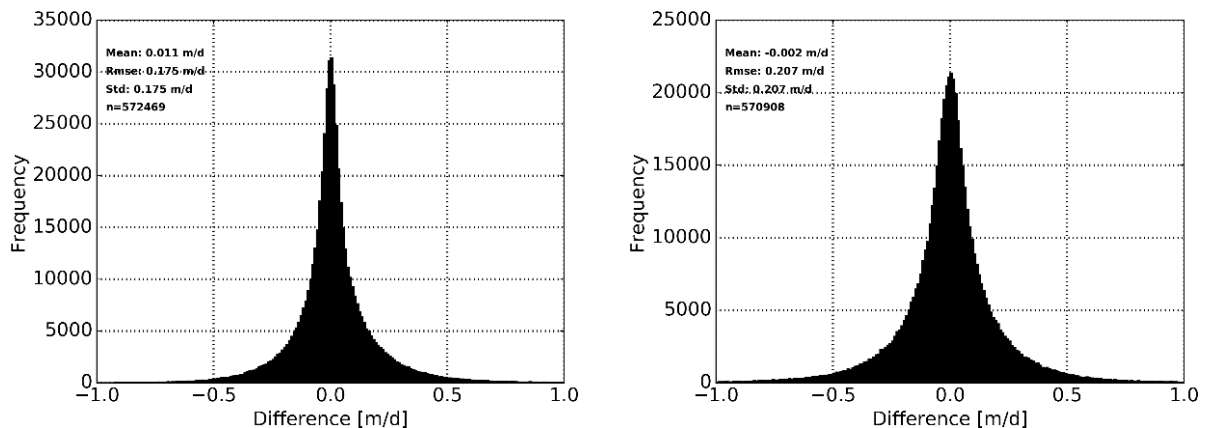


Figure 3.6: Histogram of easting (left) and northing (right) velocity residuals for the comparison of ice velocity products TSX/TDM vs. S1.

QA-IV-3 The averaged Antarctica wide Sentinel-1 IV map (period: Aug 2015-Jan 2016 & Aug 2015-April 2017) is compared with the MEaSURES (Rignot, 2011) dataset v1 & v2. The version 2 MEaSURES dataset is an update of version 1 released in April 2017. The Sentinel-1 IV map is resampled to the same pixel spacing (450m) and extend as the MEaSURES datasets. We present difference histograms and maps for both easting and northing components (Figure) including statistics (Table 3-5). The generated figures and statistics illustrate the performance and level of agreement between the IV datasets. For the intercomparison of the S1 IV map (v20160217) and MEaSURES (v1) the mean difference is 0.002 m d⁻¹ (RSME: 0.049 m d⁻¹) and 0.001 m d⁻¹ (RSME: 0.046 m d⁻¹) for the easting and northing component respectively indicating an excellent

agreement. The intercomparison of the S1 IV map (v20170428) and MEaSURES (v2) shows similar results with a mean difference of 0.001 m d^{-1} (RSME: 0.068 m d^{-1}) and 0.003 m d^{-1} (RSME: 0.067 m d^{-1}) for the easting and northing component. The difference maps show that larger deviations are concentrated in a few regions (for example Pine Island Glacier and Stancomb-Wills Ice Tongue) likely reflect actual change or might be related to different window sizes leading to differences in for example shear margins of fast glaciers.

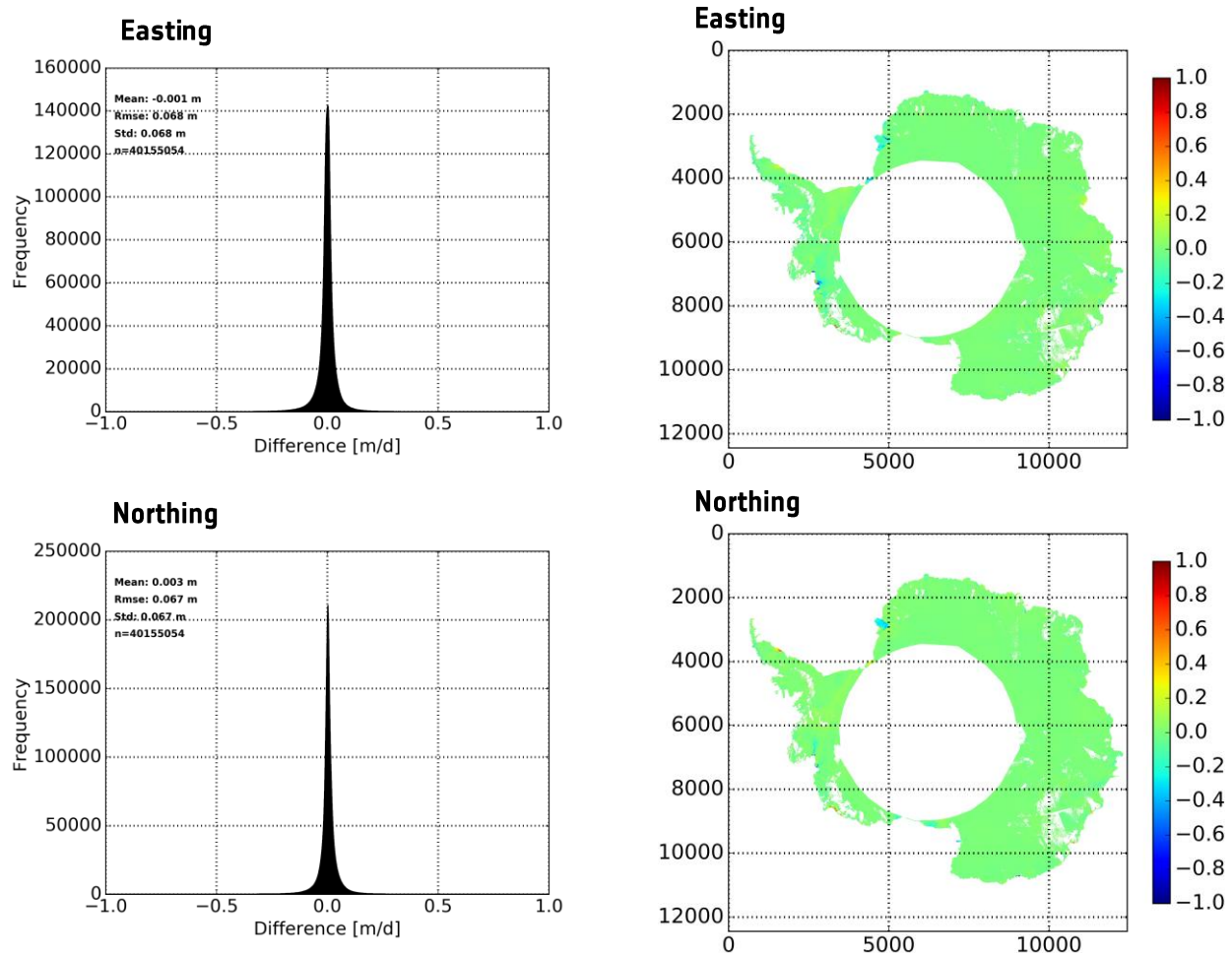


Figure 3.7: QA-IV-3: Difference histograms (left) and difference plots (right) for easting and northing component for the intercomparison between the ENVEO Sentinel-1 ice sheet wide velocity map (v20170428) and the MEaSURES InSAR-Based Antarctica Ice Velocity Map, Version 2 (Rignot et al., 2017).

Table 3-5: QA-IV-3: Summary of IV comparison quality assessment.

Products Analysed	Reference dataset	Number of pixels used in analysis	Mean difference Easting [m d ⁻¹]	RMSE difference Easting [m d ⁻¹]	Mean difference Northing [m d ⁻¹]	RMSE difference Northing [m d ⁻¹]
ais_cci_iv_s1_w 2015_v2016021 7	Measures Antarctic Velocity v1	~34.5 Million	0.002	0.049	0.001	0.046
antarctica_iv_s1_all_v20170428	Measures Antarctic Velocity v2	>40.1 Million	0.001	0.068	0.003	0.067

QA-IV-5 The stable ground test is carried out for all IV products provided that it contains ice free areas. To identify regions without motion (stable ground) vector outlines of rocks from the SCAR Antarctic Digital Database are used. In 2016 an updated rock outcrop inventory was released and included in the SCAR ADD (Burton-Johnson et al., 2016). The new inventory is based on automatic classification using Landsat 8 data and represents a major improvement over the older version. The red areas depicted in Figure (upper left panel) show the stable regions for which the analysis is performed. Layover regions are masked out and are excluded from the statistical calculations. Scatter plots and histograms are presented illustrating the distribution of the easting and northing velocity components (Figure 3.8). Ideally these should be centered at zero for stable areas. Deviations can be due to several causes including errors in the rock shapefile, errors in the layover mask and artifacts produced by the algorithm. The outcome of the stable ground test, using both the old and new ADD versions, are summarized in Table 3-6. Results indicate on average a mean of $<<0.01 \text{ m d}^{-1}$ and an RMSE $< 0.03 \text{ m d}^{-1}$ for both easting and northing velocity components). The use of the updated rock outlines is primarily reflected in a significant reduction of the RMS in the order of 35-45% for both easting and northing components.

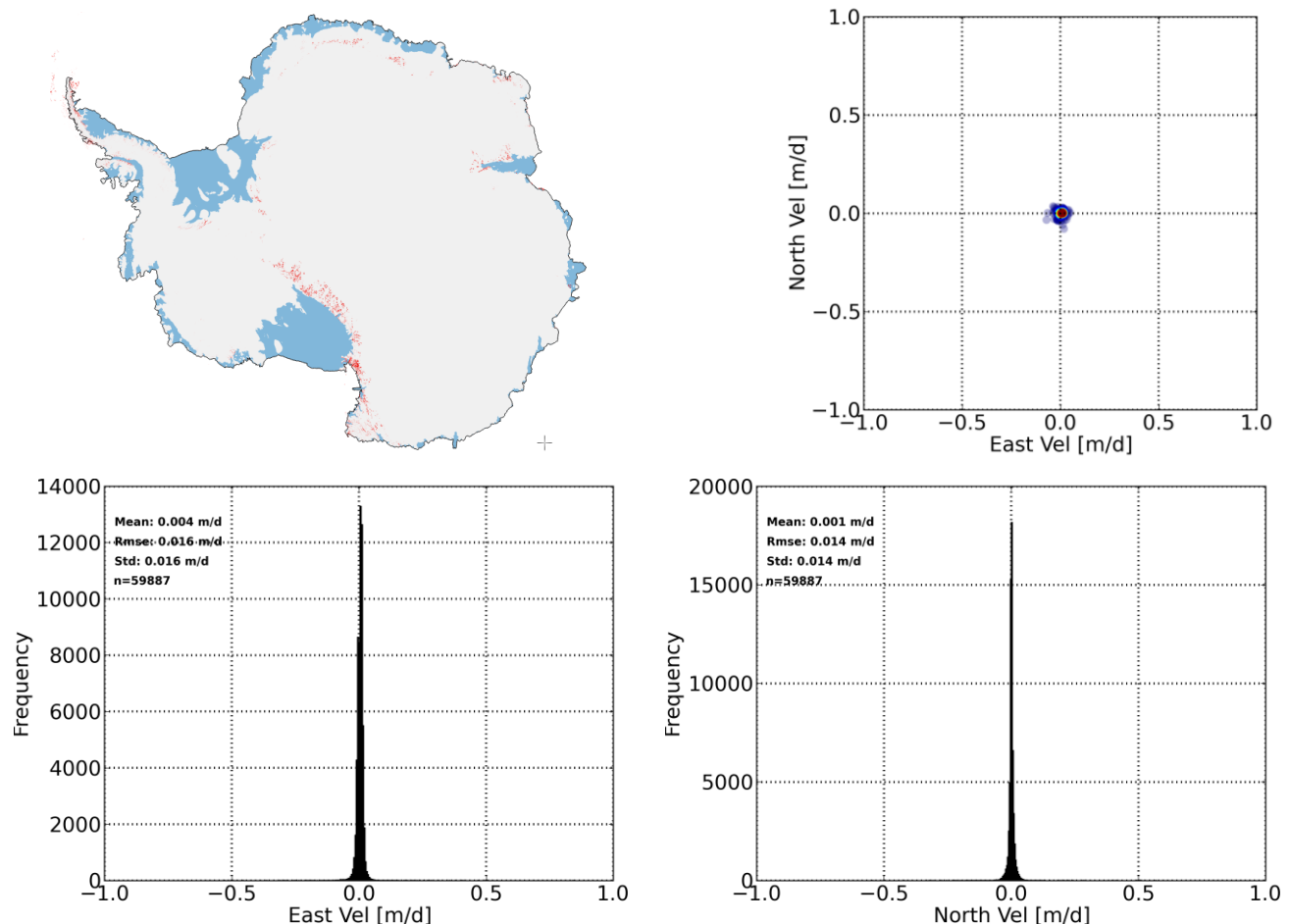


Figure 3.8: Results of the stable rock test. Upper left panel: stable rock area used in the analysis depicted in red. Upper right panel: scatter plot showing easting velocity versus northing velocity with colour coding blue to red indicating point density from low to high. Lower left panel: histogram of easting velocity. Lower right panel: histogram of northing velocity.

Table 3-6: Summary of stable rock quality assessment for averaged S1 ice velocity map (v20160217).

Rock Database	Number of pixels	Mean E [m d⁻¹]	RMSE E [m d⁻¹]	Mean N [m d⁻¹]	RMSE N [m d⁻¹]
ADD (old)	100,127	0.004	0.024	0.002	0.025
ADD (Burton-Johnson et al., 2016)	59,887	0.004	0.016	0.001	0.014

4 Grounding Line Location (GLL)

This chapter gives a complete report of the activities carried out to assess the quality of the GLL products.

4.1 Independent validation data

Requirements

The boundary of the grounded ice sheet includes a variety of structural conditions:

- glacier tongues (ice thickness gradually decreases)
- ice cliffs (ice breaks off and falls onto the ground or sea ice)
- ice shelves (ice flows into the ocean and remains attached to the grounded ice until it calves). This is the dominant situation in Antarctica, stretching about 19,000 km in length (British Antarctic Survey, 2005).

For the most cases, e.g. an outlet glacier with a floating tongue or on an ice shelf, the GLL is not directly observable. Therefore the validation of the GLL outcome of the present AIS_cci project will be carried out against similar products consisting of indirectly derived GLLs from a variety of satellite data and the appropriate indirect method.

Although within AIS_cci we do not aim at deriving the GLL on a continental scale we selected the most commonly used Antarctica-wide GLL databases available for download at NSIDC for validation. A detailed description is given in Section 0.

In order to facilitate the intercomparison of the various GLLs, the AIS_cci GLL product is annotated with time stamps and ocean tide level differences. Since this information is not given for the validation datasets an interpretation of the comparison must be done with care in particular with respect to GLL migration. Therefore at the current stage of the project we limit our comparison to a purely geometrical/spatial approach which does not take ocean tide changes into account. Another issue which needs to be considered in conjunction with that topic is the subglacial topography. This will be examined in future updates of this document.

Sources

Three comprehensive data sets were used to validate the AIS_cci GLL. Their details are given below.

- (1) The Antarctic grounding line derived from the MODIS Mosaic of Antarctica (**MOA**) from (Scambos et al, 2007)

This GLL was generated together with the coastline from the digital image mosaic of surface morphology assembled from 260 Moderate-resolution Imaging Spectroradiometer (MODIS) images acquired between Nov. 2003 and Feb. 2004. The good geolocation and slope sensitivity of the MOA surface morphology image made a continent-wide mapping of the coastline and the grounding line possible. In (Scambos et al, 2007) the grounding line is defined as the coastal slope break between floating and grounded ice (I_b in Figure). The GLL was manually digitized by following the seaward-most continuous slope break on the surface inside of (or equal to) the permanent coastline in images of the MOA surface morphology dataset.

The coastline and the grounding line are two vector files which can be downloaded at ftp://sidacs.colorado.edu/pub/DATASETS/nsidc0280_moa2004/coastlines/ in various formats. The spatial resolution is 250 m. The location precision is estimated to be no

worse than ± 250 m. The MOA grounding line is the only available dataset which has a 100% complete coverage including continent and islands. The time stamp (date/time) of the MODIS acquisitions used to generate the MOA grounding line segments is unfortunately not given.

(2) The Antarctic Surface Accumulation and Ice Discharge (**ASAIID**) IPY project, from (Bindshadler et al. 2011)

Two ice-dynamic features were mapped within this project: the seaward boundary of surface morphology associated with grounded ice (I_b in Figure) and the landward boundary of freely floating ice shelves or hydrostatic line (H in Figure). The boundaries were generated at a spatial resolution of 15 m from Landsat-7 imagery acquired between 1999 and 2003 and ICESat/GLAS laser altimetry from two observation periods in 2003 and 2008. The photogrammetry procedure is based on the relationship between the pixel brightness in the optical image and the surface slope. In addition an ICESat/GLAS elevation (up-sun and down-sun) is required in order to delimitate the subimage where the brightness-slope relationship is applied. The authors mention that identifying where the fast moving glaciers discharge into ice shelves was the most challenging task. In these cases additional MOA imagery is analysed and at all locations where the MODIS shows additional grounded ice features it will be compared to Landsat. Here the ASAIID GLL follows the MOA GLL.

The grounding line and hydrostatic line locations can be downloaded at http://nsidc.org/data/docs/agdc/nsidc0489_bindshadler/. The spatial resolution is 15 m. The positional accuracies of the ASAIID GLL vary from ± 52 m for the land and open ocean terminating segments to ± 502 m for the outlet glaciers. The hydrostatic line (H) is positioned with errors of over 2 km. The ASAIID GLL is consistent around the continent, but covers only 3 islands. The time stamp (date/time) of the Landsat-7 acquisitions used to generate the ASAIID GLL segments is not given.

(3) The **MEaSURES** InSAR grounding lines from (Rignot et al. 2011)

This GLL product consists of the mapped upper limit of tidal flexure (F in Figure) observed in differential interferograms (DInSAR) around Antarctica. The satellite data used are ERS-1/2 from 1992, 1994 and 1996, RSat-1 from 2000, RSat-2 from 2009 and ALOS PALSAR from 2007-2008 extending over a large time span for more than 15 years. The DInSAR technique to obtain the distinct signature of elastic bending is the same as that used in the present AIS_cci project. The GLL was manually mapped in the SAR geometry and georeferenced afterwards.

The grounding line can be downloaded at <https://nsidc.org/data/nsidc-0498>. The spatial resolution is 50 m. The standard deviation of the errors is ± 100 m and was found from comparison with multiple mappings, instruments and epochs (including the MOA grounding line). Locally greater variations are observed. In some cases km-wide migrations were detected.

The coverage is incomplete in some areas (due to the lack of coherence) while in other areas multiple inner flexure lines (F) were obtained at different dates. The time stamp (date/time) of the SAR acquisitions used to generate the MEaSURES GLL segments is annotated in the product which is helpful if ocean tide levels shall be extracted for comparison later.

Assessment

Although the term “grounding line” is generally used to define the boundary of the grounded ice sheet and a floating ice shelf it can be applied to various datasets using different methodologies sensitive to different topographic or dynamic features. In order to avoid confusion when the different grounding line products are compared with the AIS_cci GLL the processes and features at the margin of the ice sheet are schematically outlined in Figure and will be discussed in the following.

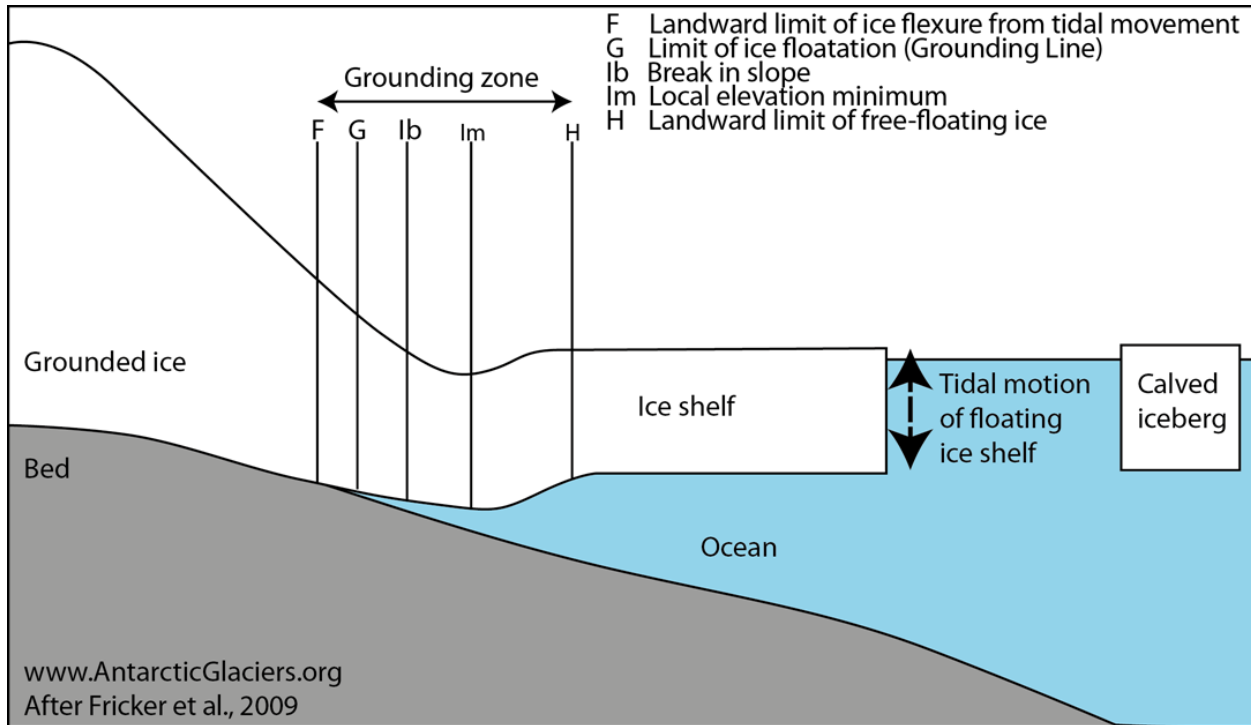


Figure 4.1: Processes and features at the grounding zone.

The grounding zone extends between the point F, the most seaward point not vertically displaced by tidal flexure, and H, the most landward location that experiences vertical motion equal to the magnitude of the ocean tide. G is the location where the ice loses contact to the bed (at low tide). I_b and I_m are inflections of the surface slope where the slope changes most rapidly (break in slope) and where the slope is zero, respectively. Different techniques determine different points within the grounding zone. H is not well known, but F and I_b have been extensively mapped.

The MOA and ASAD grounded ice boundaries (GLLs products) are most consistent with point I_b, the slope break. SAR sensors detect the band of flexure between F and H which appears as a typical pattern of dense fringes in the double difference interferograms. Although F is not identical with G, since F and G lay very close together (< 1 km) (Rignot et al. 2011) the upper limit of flexure is treated as GLL. This is the case for MEaSUREs and AIS_cci (see RD4) products. Repeat laser altimetry can detect H and F from repeat-track analysis and I_b and I_m from single profiles (Bindshadler et al. 2011).

The zone F-H is typically 2-11 km wide on Antarctic glaciers but can also reach extreme values of up to 25 km in areas that are lightly grounded or where tidal flexure is highly contorted by boundary conditions. I_b is typically a few km downstream of G.

Selection

The AIS_cci grounding lines are validated against the independent datasets described in Section 0. The comparison is carried out on four areas (Figure 4.2). Additionally, the Schirmacher site has been divided into one area covered by Sentinel-1 and one area where ERS-1/2 data was used.

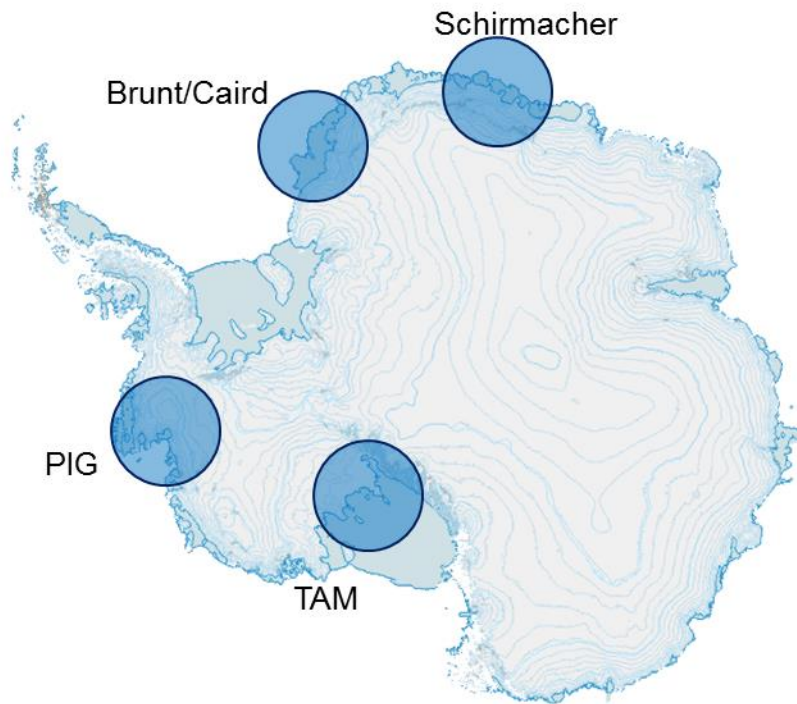


Figure 4.2: Validation test areas for the AIS_cci GLL products: Schirmacher, Brunt/Caird, PIG – Pine Island Glacier and TAM – Transantarctic Mountains.

4.2 Validation procedure

For the validation, the GLLs are compared with a spatial metric. A tide level dependent comparison is a goal for further comparisons later in the project but it is currently difficult to perform since no exact acquisition times are given in the other datasets. Using MEaSURES date stamp and orbit number theoretically allows the determination of the actual acquisition time required for tide prediction. However, since this is a rather extensive task, it cannot be performed within the first year PVIR.

We carry out our analysis in four areas and compare AIS_cci GLLs with each of the GLLs described in the validation set (Section 0). If there is more than one GLL in a specific validation product all of them will be analyzed, since no temporal separation is currently performed.

The different GLL datasets are referenced as:

Reference	Description
AIS_cci	Our product derived from interferometric data
ASAID	ASAID GLL

MOA	MOA GLL
MEaSURES	MEaSURES GLL

All GLLs superimposed on the RSat-1 SAR backscattering mosaic are shown in Figure 4.3 to Figure 4.7. A first visual comparison suggests a good overall agreement between all GLL products within a range of 5 km to 10 km.

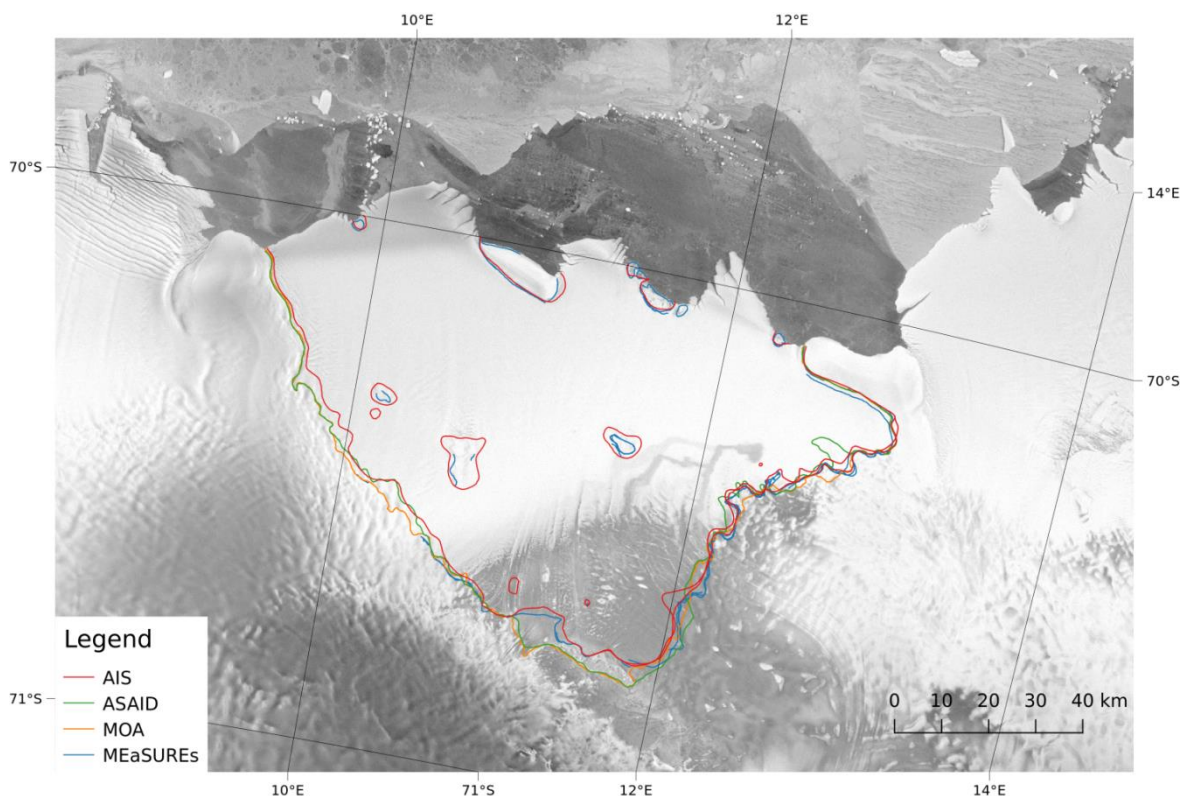


Figure 4.3: The Schirmacher ERS area (Nivlisen Ice Shelf) with all validation GLLs and the AIS GLL derived from ERS-1/2 data.

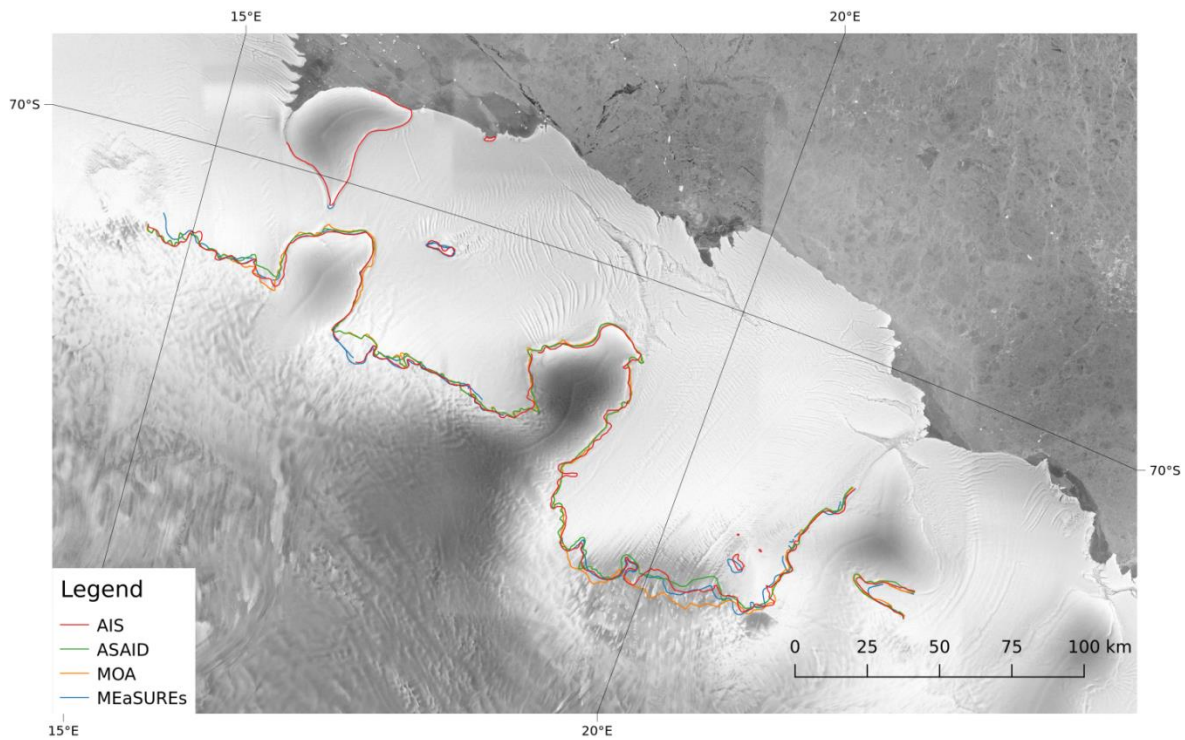


Figure 4.4: The Schirmacher S1 area (Lazarevisen Ice Shelf) with all validation GLLs and the AIS_cci GLL derived from Sentinel-1 data.

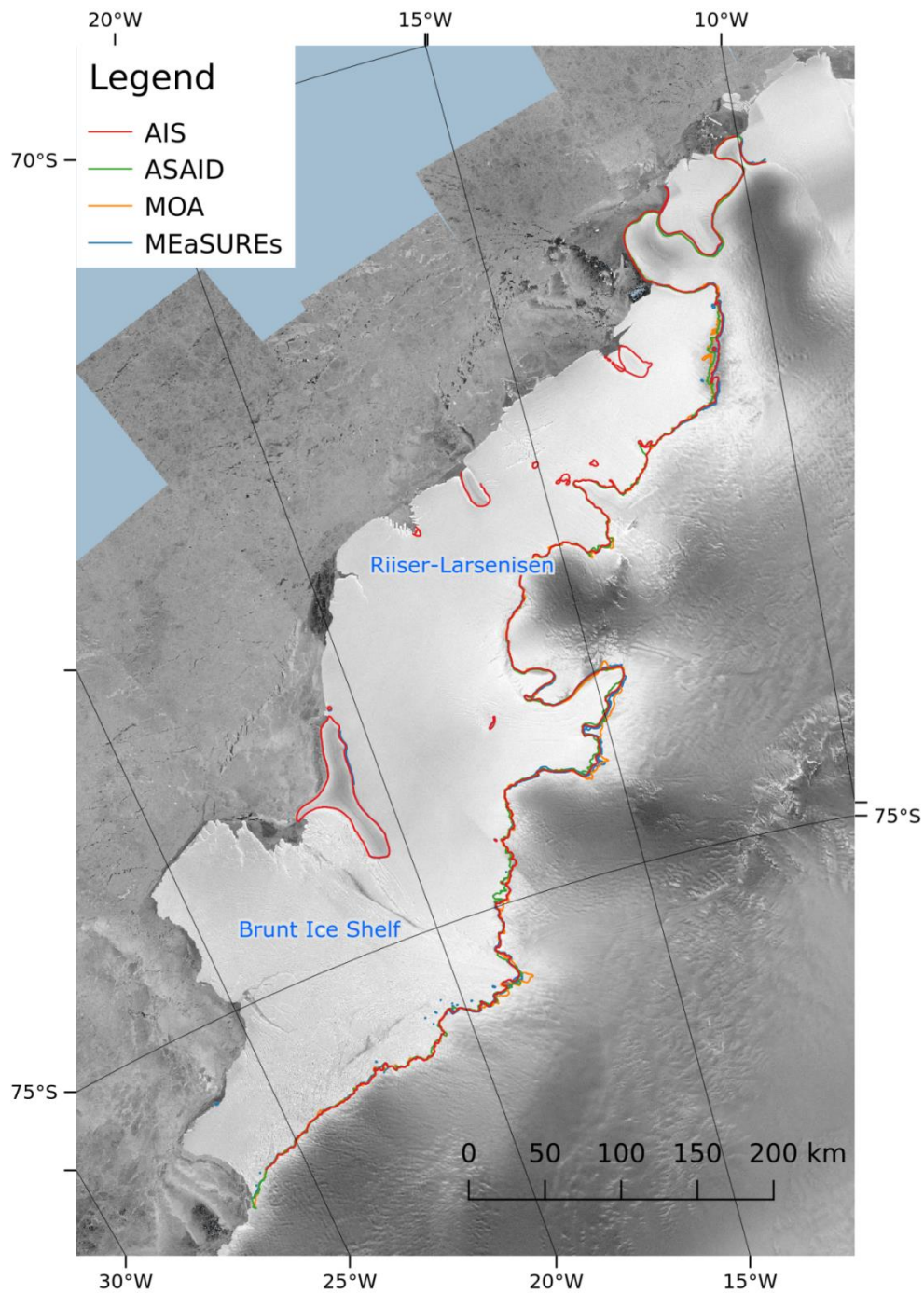


Figure 4.5: The Brunt Ice Shelf/Caird Coast area (incl. Riiser Larsenisen Ice Shelf) with all validation GLLs and the AIS_cci GLL derived from ERS-1/2 data.

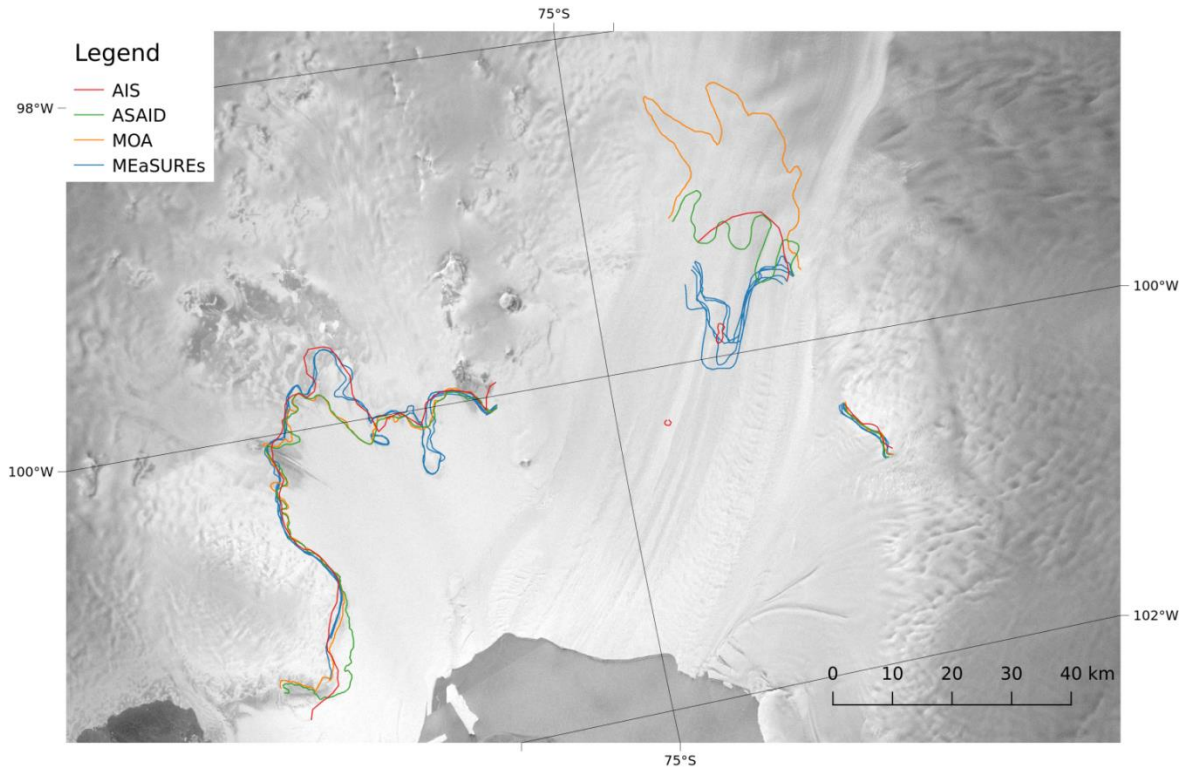


Figure 4.6: The PIG area with all validation GLLs and the AIS GLL derived from ERS-1/2 data.

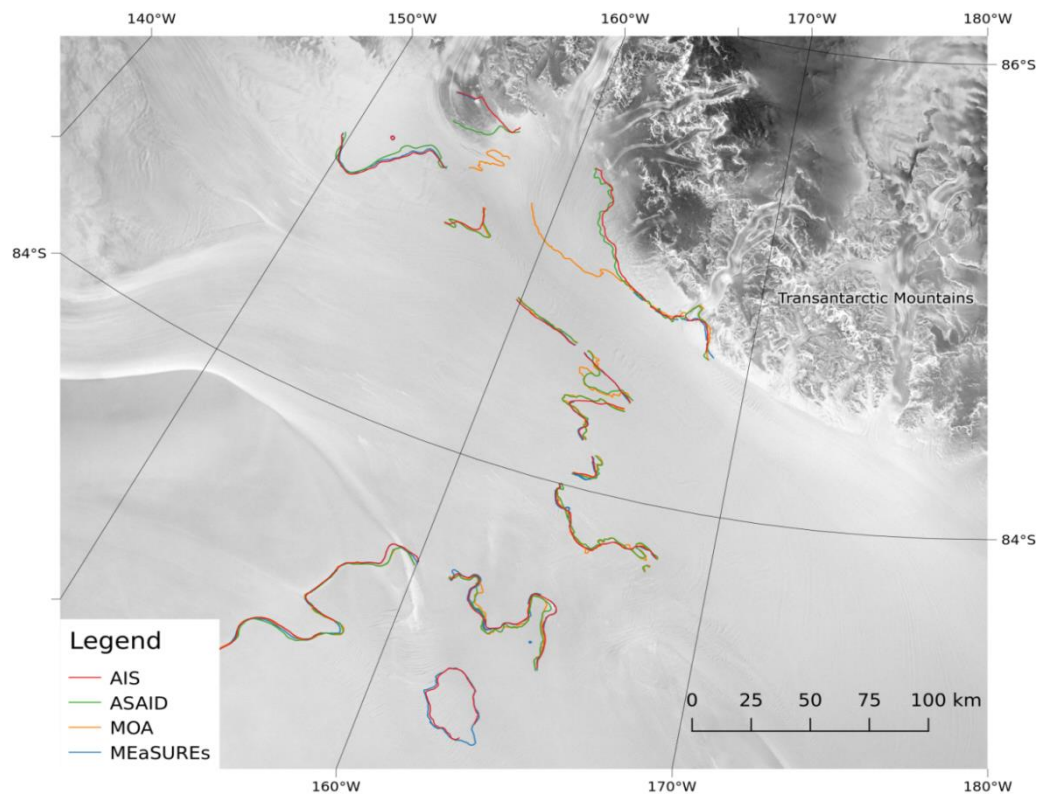


Figure 4.7: The TAM area (Southern Ross Ice Shelf and Transantarctic Mountains) with all validation GLLs and the AIS_cci GLL derived from TerraSAR-X data.

In order to quantify the differences among the various GLLs a polygon comparison procedure has been adapted to project's needs and has been implemented for the purpose of validation. All selected validation lines and our product are represented as two-dimensional polylines. Polyline is a collection of points with a defined connection.

A problem which occurs if two polylines are compared is that there is no defined mapping between the points belonging to the reference line and those belonging to the target line, respectively. Moreover, the sampling of both polylines may differ significantly. This implies that a distance between points cannot automatically be calculated for each point without defining a line-to-line (or point-to-point) assignment. One solution which provides a mapping between two lines is the assumption that for each point on the target line, the closest point found on the reference line is the corresponding point. It is important to note, that even if the same mapping technique is used the result of the assignment may vary depending on which lines are selected as target and reference, respectively.

A good way to visualise minimal distances around a line is to create a region around it, we call this object a buffer. One example of using a buffer around a polyline is shown in [Figure 4.9](#). The buffers around the AIS_cci GLL, defined as reference line, are increased until the target line (ASAID GLL) is completely contained within the buffer (e.g. at 5000 m distance). The overlap with the target line can be calculated for each buffer distance. These buffers can then be used to calculate the overlap (expressed in percentage) with other lines at a specific distance.

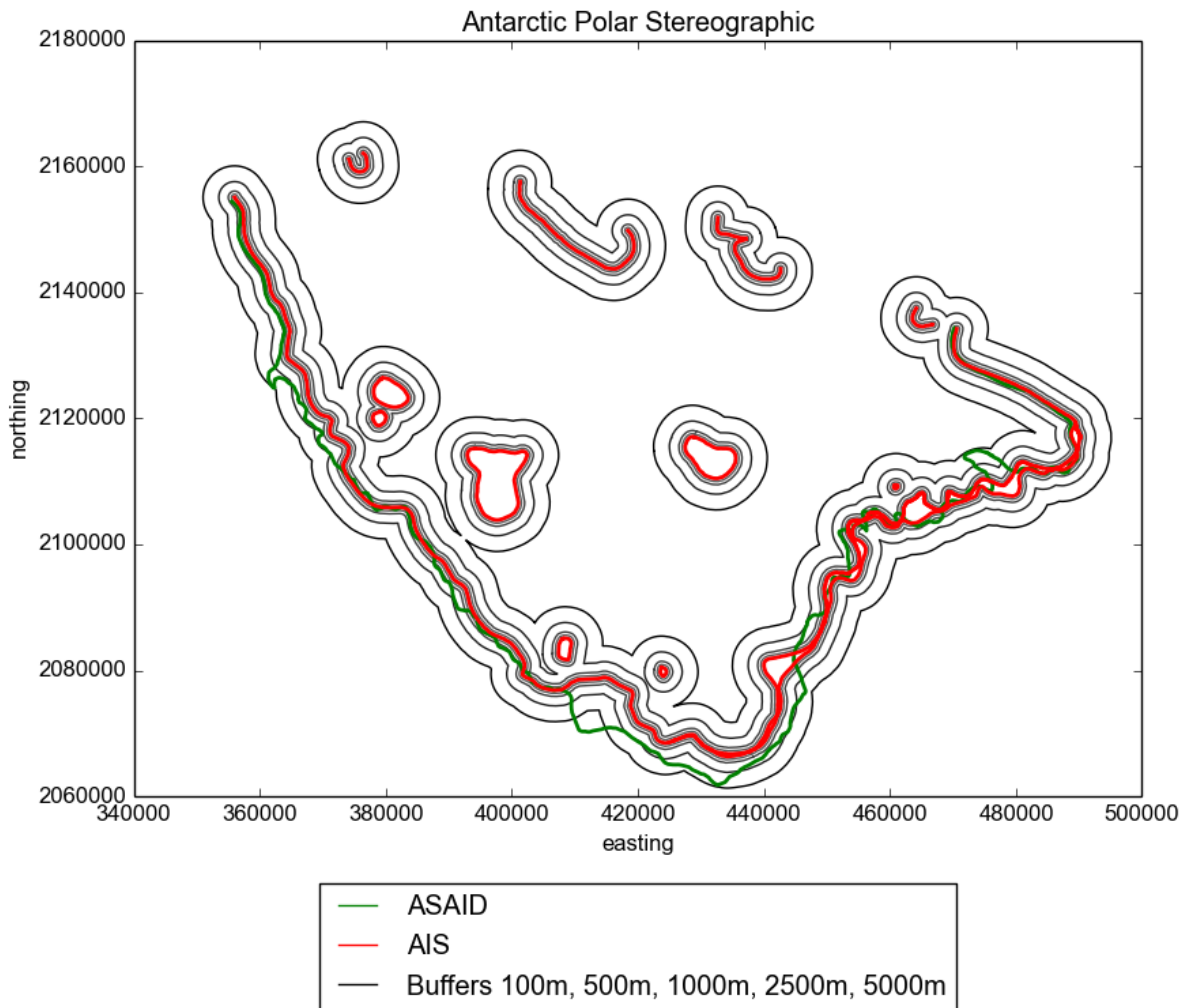


Figure 4.8: Buffers (black lines) corresponding to different distances around the AIS_cci GLL (reference line, in red). The target line is the ASAID GLL (in green). At the largest distance of 5000m the green line is almost completely contained within the buffer.

very small steps in order to get more precise results. Because of this we decided for a more generic approach – a proximity image – which is simply another implementation. The reference polyline is represented in a binary image and the shortest distance for each pixel in the image to the reference line is determined and stored as value at this point. The spatial sampling of that image is 5 m x 5 m which therefore is the smallest detectable difference. Such a proximity image is shown in Figure 4.10.

All datasets which shall be validated are now equally resampled and superimposed onto this image. Depending on the shape of the polyline these datasets will cross different “distance values” of the proximity image. All the values which will be encountered if one traverses along the GLL of the validation dataset result in a histogram (left side plots on Figure 4.11 to Figure 4.15). The more values obtain shorter distances, the better the final fit will be. Besides the histogram characteristics, the mean values of the distances also quantify the equality between two polylines and are given in Table 4-1.

In order to show how well the target lines are approximated by the AIS_cci we also determine, how much of the other curve is covered by the reference curve within a predefined buffer size. This step is repeated for different continuously growing buffer

sizes. A plot of the overlap (in percentage) against the buffer size is generated for each of the target lines in each of the validation sites. This is called a Cumulative Ratio Curve (CRC) and is similar to a Cumulative Density Function of a distribution (Heo 2009), (Jeong 2013). The CRCs are shown on the right side plots of Figure 4.11 to Figure 4.15.

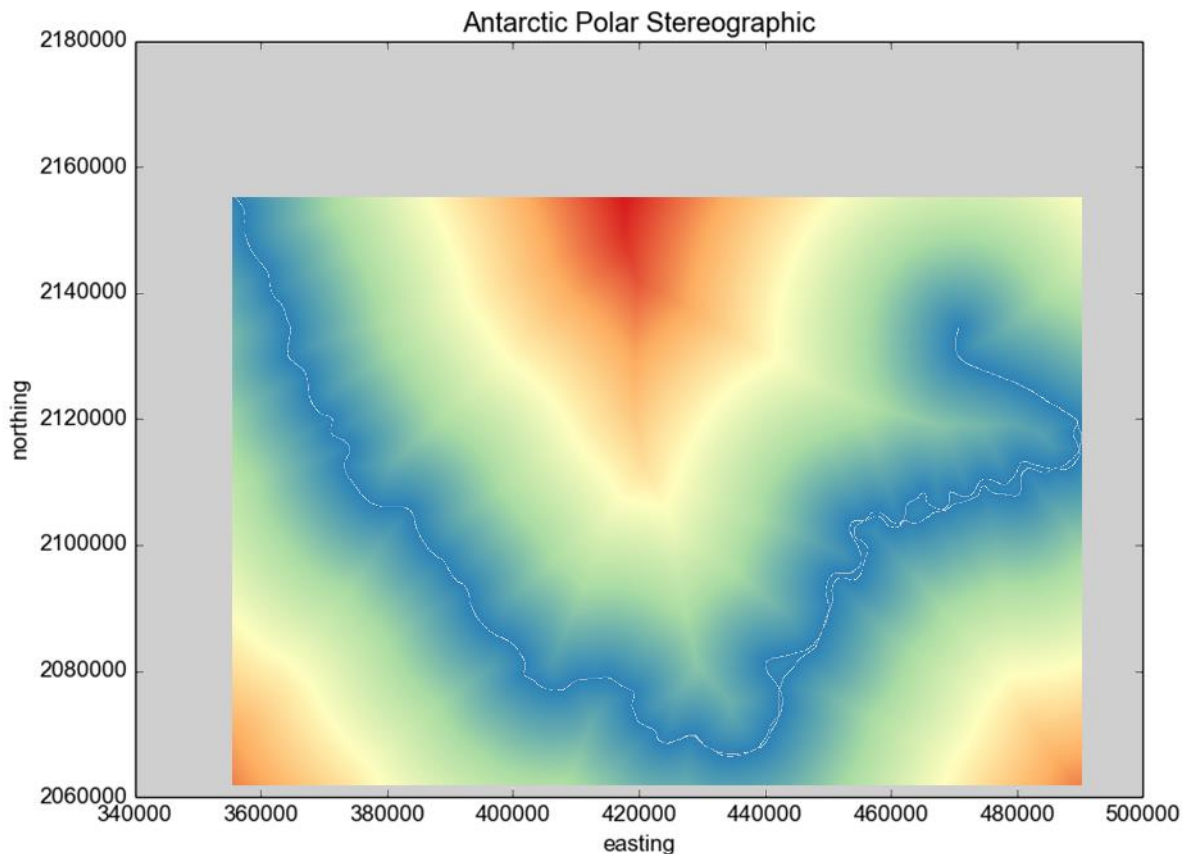


Figure 4.10 Proximity image for AIS_cci GLL at Schirmacher derived from ERS. The color scale from blue-green-yellow-red depicts increasing distances to the polyline. The white line is the reference AIS_cci GLL.

4.3 Validation outcome

We performed the validation procedure on each of the four areas by comparing the AIS_cci GLLs with the independent validation dataset. Each comparison yields an average minimal distance between the lines which represents the mean value of "difference" between the participating lines (Table 4-1). For each comparison the histograms and CRC curves described in Section 4.2 were generated (Figure 4.11 to Figure 4.15). In addition we compared a segment of the grounding line which was generated from the same SAR dataset within two different projects, MEaSURES and AIS_cci (Section 0).

Table 4-1: Mean of the distances between the AIS_cci GLL and the respective validation candidates.

	d _{ASAID} [m]	d _{MOA} [m]	d _{MEaSURES} [m]
Schirmacher ERS	1372	1481	599
Schirmacher S1	782	1056	688
Brunt/Caird	666	953	446
PIG	1871	5625	3649
TAM	2039	4016	573
Average (all areas)	1328	2626	1191
Average (excl. PIG)	1215	1877	576

In the PIG area the mean distances AIS_cci vs. MEaSURES have to be interpreted with care because the MEaSURES dataset contains a time series of GLLs which vary significantly in locations (up to 12 km). In this case the overlap ratio is < 1 even for big buffer sizes and reaches 1 at distances much larger than the 5000 m.

Schirmacher area

Schirmacher ERS

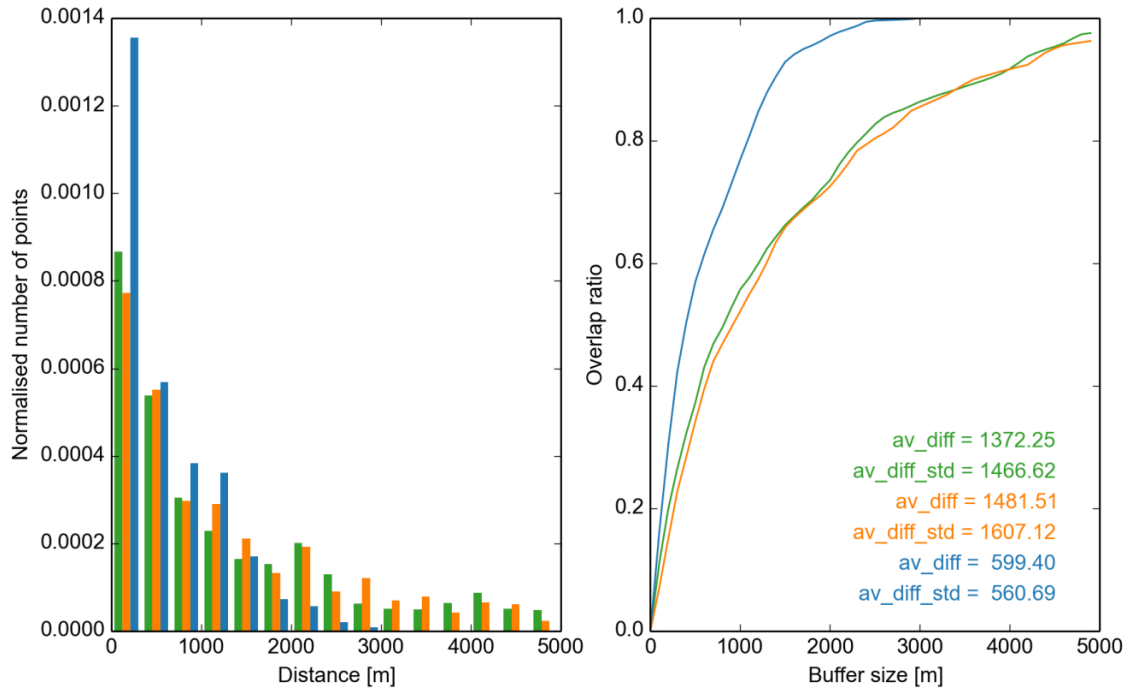


Figure 4.11: Comparison of the AIS_cci GLL line in the Schirmacher area derived from ERS data with the validation GLL: AIS_cci vs. ASAlD (green), MOA (orange) and MEaSURES (blue). Left: histogram of the distances between the GLL lines. The number of points is normalised with respect to the area below the curve. Right: the Cumulative Ratio Curve.

Schirmacher Sentinel-1

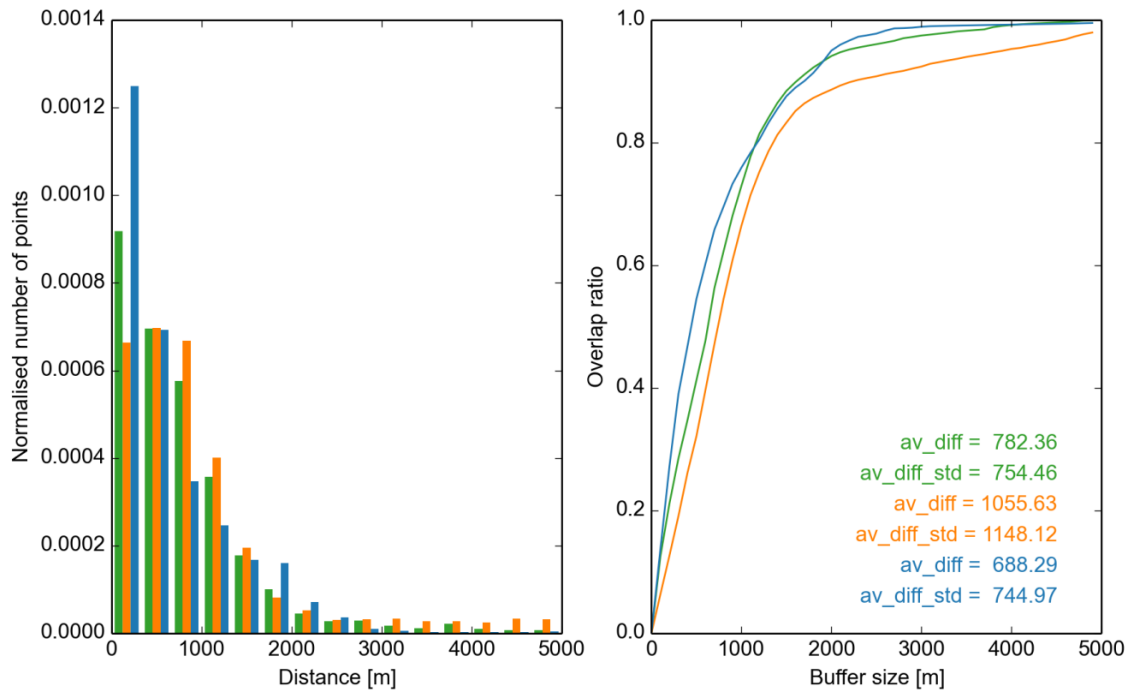


Figure 4.12: Same as Figure 4.11 but in the Schirmacher area. The AIS_cci GLL was derived from Sentinel-1 data.

Brunt/Caird

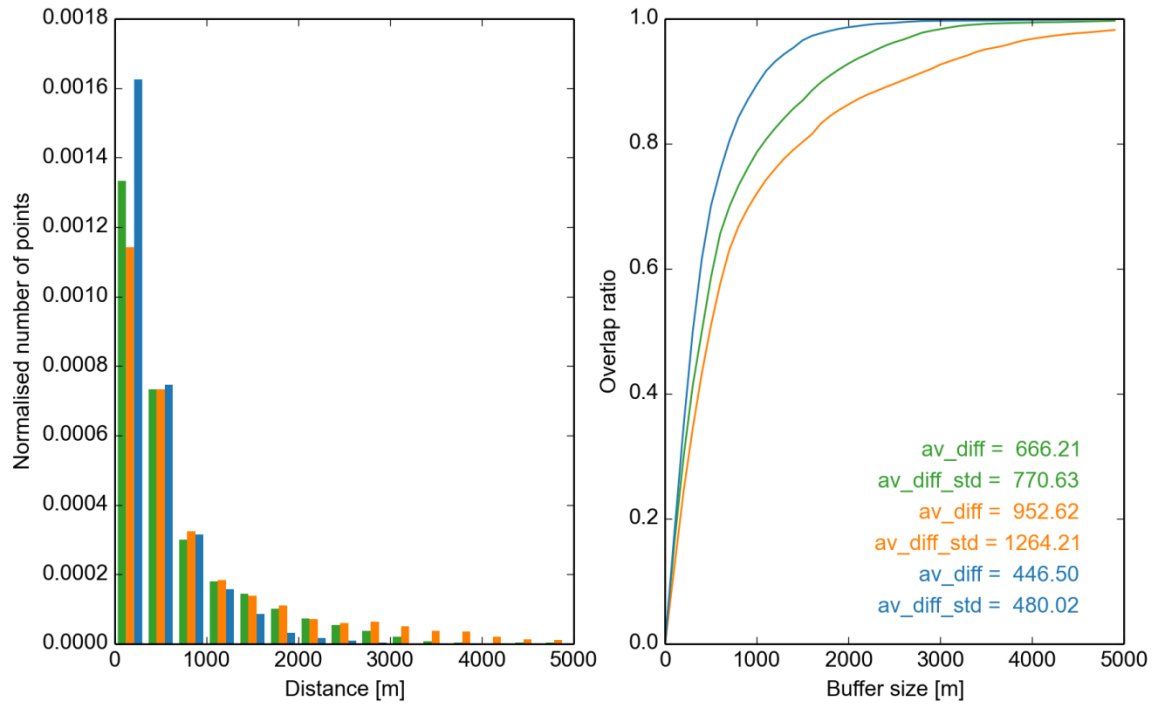


Figure 4.13: Same as Figure 4.11 but in the Brunt/Caird area. The AIS_cci GLL was determined from ERS-1/2 data.

PIG

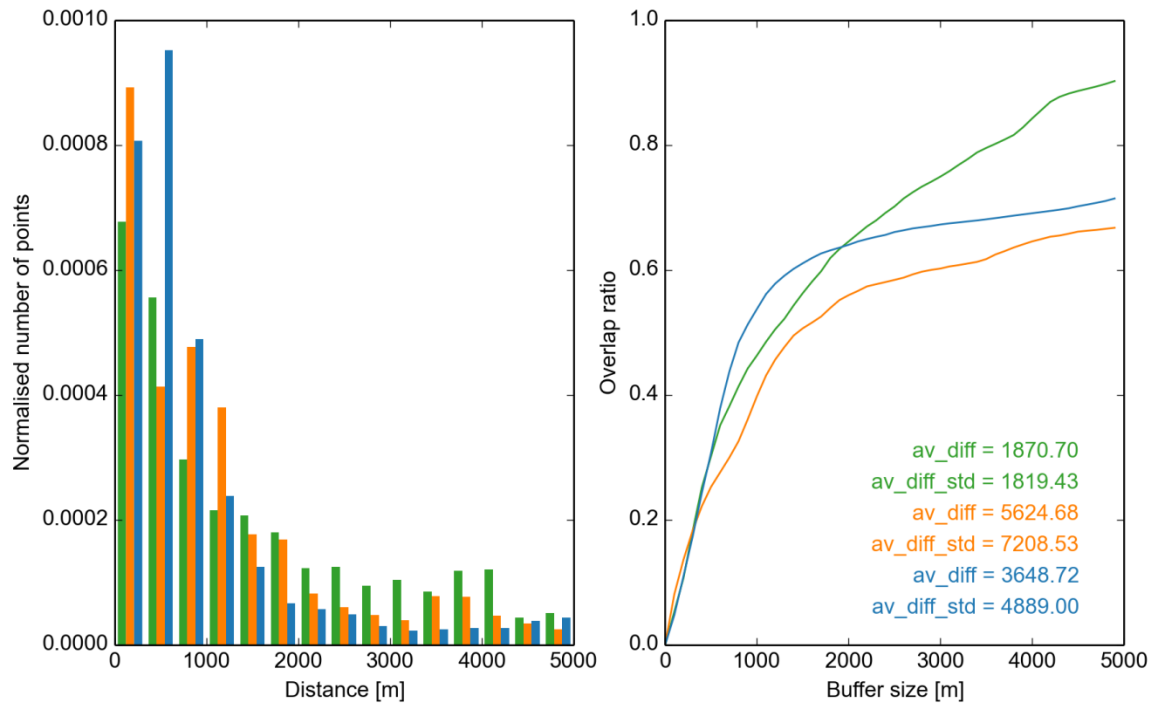


Figure 4.14: Same as Figure 4.11 but in the PIG area.

TAM

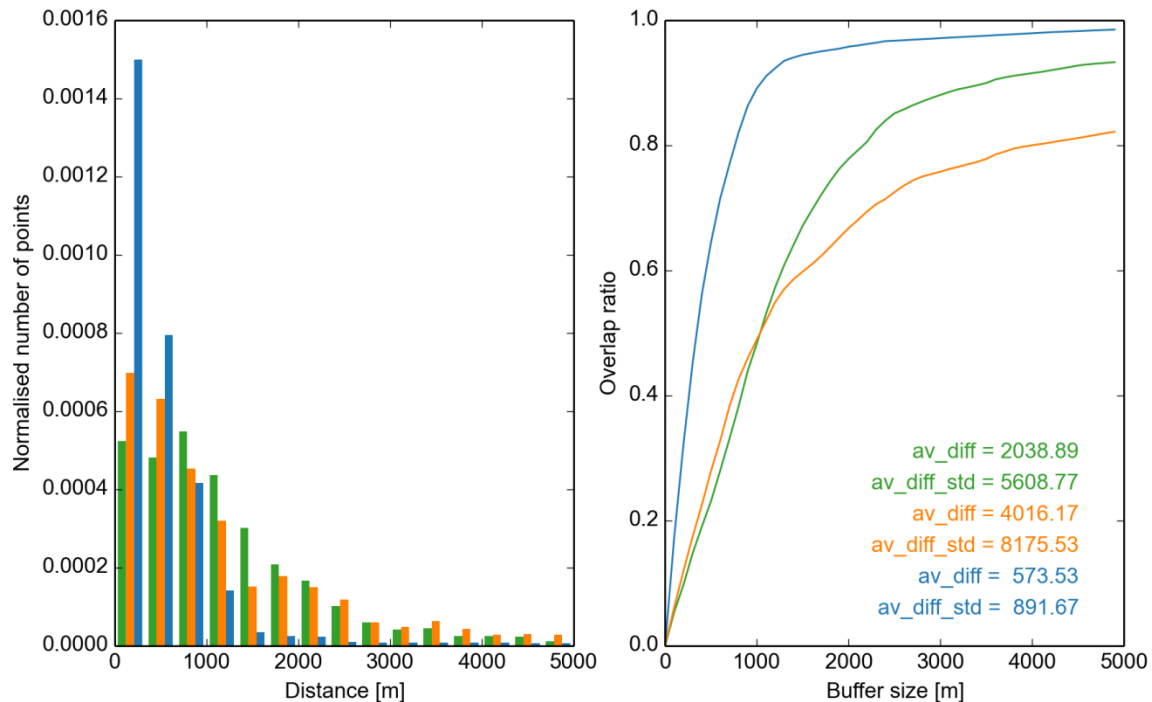


Figure 4.15: Same as Figure 4.11 but in the TAM area. The AIS_cci GLL was obtained from TerraSAR-X data.

Identical SAR datasets: MEaSURES vs. AIS cci

For a validation that takes temporal variation of the GLL into account, we compare two AIS_cci GLLs against grounding lines generated within the MEaSURES project (Rignot et al, 2011), (Scheuchl et al, 2016). In contrast to the comparisons shown above, this validation only concerns grounding line segments that have been produced from identical SAR acquisitions. In particular, we carry out two comparisons:

1. both AIS_cci and MEaSURES GLLs were created from Sentinel-1A satellite data acquired on the dates 2014-11-23, 2014-12-05 and 2014-12-17 (Figure 4.15 a)
2. both AIS_cci and MEaSURES GLLs were created from ERS-1 satellite data acquired on the dates 1994-03-04, 1994-03-07 and 1994-03-11 during the 2nd Ice Phase (Figure 4.15 b)

By using the identical SAR acquisitions, temporal variations between AIS_cci GLLs and MEaSURES GLLs due to tide level variations or grounding line retreat are excluded. The differences of the GLLs reflect the spatial accuracy of the grounding line delineation using the same methodology. Therefore, we expect smaller mean differences between these GLLs than in the comparison of the validation GLL products presented in sections 0 to 0. From the visual inspection in Figure 4.15 it is obvious that both AIS_cci and MEaSURES GLLs are overlapped well on Dotson/ Crosson Ice Shelves and Jutulstraumen Glacier. Just in some areas on Dotson/ Crosson Ice Shelves neither AIS_cci GLL nor MEASURE GLL could be derived.

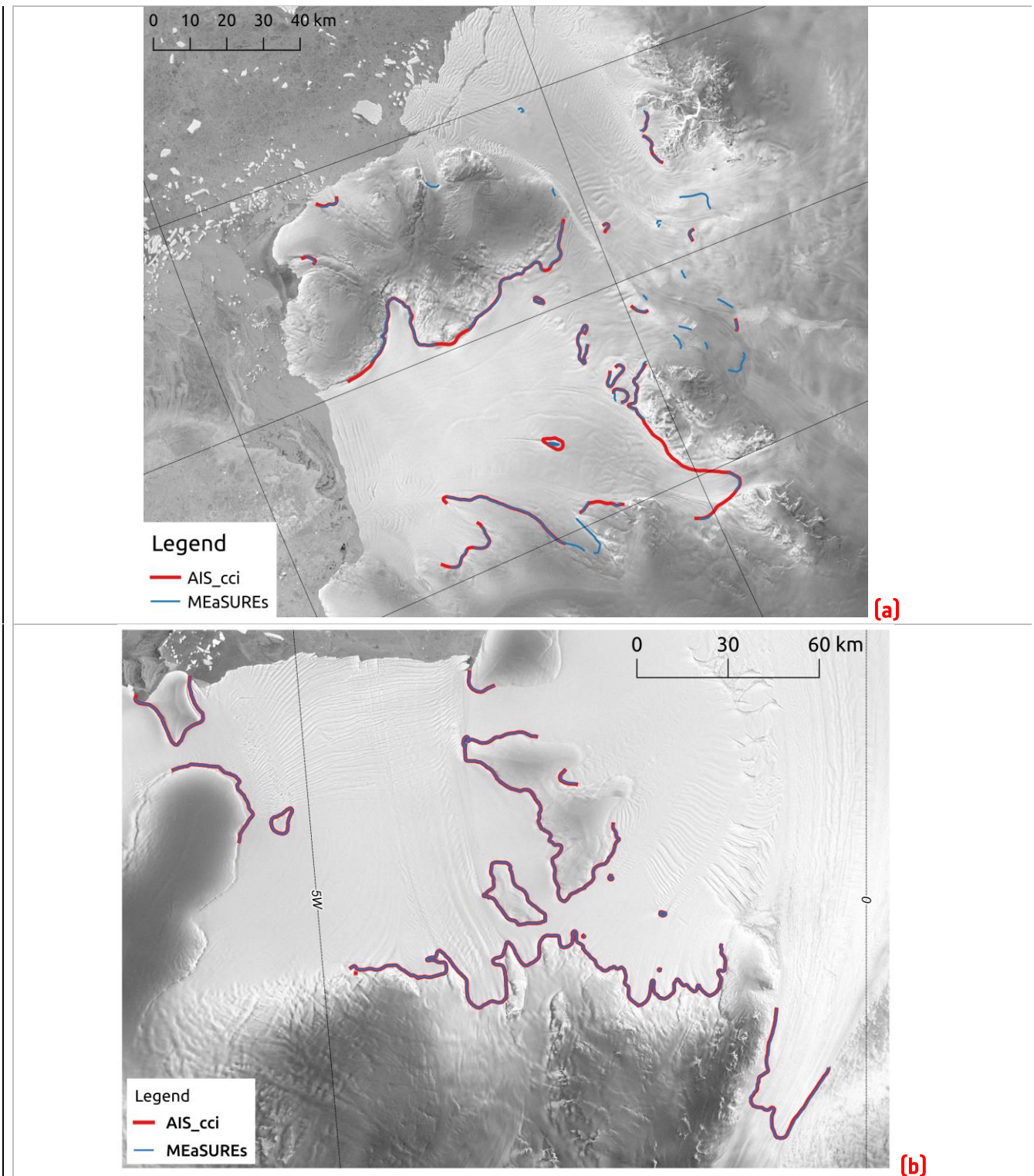


Figure 4.16: AIS_cci (red) and MEaSUREs (blue) GLL segments in (a) the Dotson/Crosson Ice Shelves area generated from the Sentinel 1A data triplet acquired on 2014-11-23/ 2014-12-05/ 2014-12-17 and (b) Jutulstraumen Glacier area generated from the ERS-1 triplet acquired on 1994-03-04/ 1994-03-07/ 1994-03-11.

We use the same methodology that was applied in the previous comparisons as a metric to report spatial differences of the GLLs. This time however, the comparison is done bidirectional, meaning that distances from each point defining the AIS_cci GLLs to the MEaSUREs GLLs are calculated and vice versa. The full comparison results are shown in Figure 4.17 to Figure 4.19. In Figure 4.17 all GLL segments, which are generated from identical Sentinel-1A triplet, are compared to each other even if they

don't have a matching counterpart in the other dataset, while in Figure 4.18 and Figure 4.19 only GLL segments derived from Sentinel-1A and ERS-1 showing in both datasets are compared.

The two GLL products are following each other very well. Within a 500m buffer distance around the AIS_cci GLL 79% of the MEaSUREs GLL can be explained (red line in Figure 4.17 right). The fact that this ratio doesn't increase significantly with a growing buffer size means that about 20% of the MEaSUREs GLL has no matching counterpart in the AIS_cci dataset.

Similar is observed for the MEaSUREs GLL that has about 76% overlap with the AIS_cci dataset within the first 500m (blue line in Figure 4.17 right). The overlap increase at higher buffer distances is due to the fact that missing parts of the MEaSUREs dataset are often a continuation of the lines detected in AIS_cci GLL, whereas the parts that are missing from the AIS_cci dataset mostly stem from individual MEaSUREs GLL segments that are often far from other GLLs (see Figure 4.15 a).

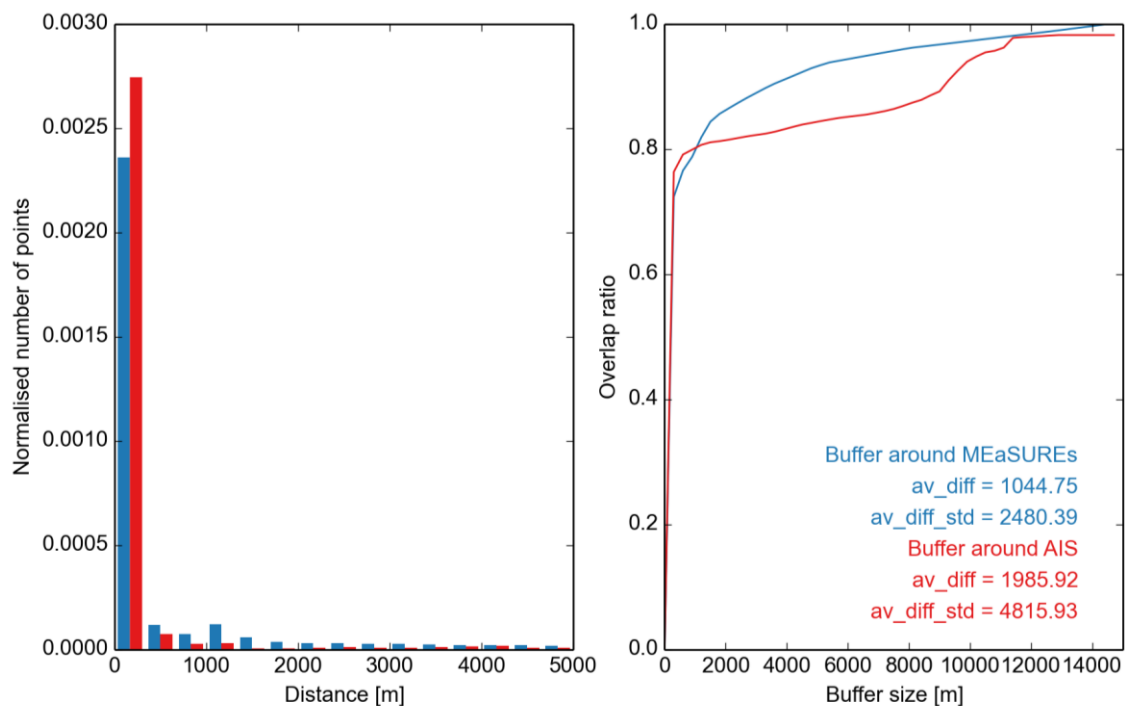


Figure 4.17: The bidirectional comparison results for GLL from identical Sentinel-1A acquisitions. All line segments are compared to each other. Left: histogram of the distances between the GLL lines. Right: Red line results when the distance from each point of MEaSUREs GLL to the closest point of AIS_cci GLL is calculated. Blue line results when the distance from each point of AIS_cci GLL to the MEaSUREs GLL is calculated.

To better assess the similarity of both GLLs, we only include GLL segments that have a mean distance of less than 5000m to its closest counterpart and therefore disregard line segments that don't have a matching representation in the other dataset. In Figure 4.17 we show the results and report mean distances of 129 and 173m for the two directions of comparison, respectively. As expected there is now an almost complete overlap of the GLLs within small buffer distances. The remaining non-overlap is caused by line segments which have a small mean distance and are therefore included in the comparison, but that contain a number of points that have no matching counterpart. These are mostly line continuations where one candidate ends earlier than the other.

In Figure 4.19 the comparison is done between the GLLs which are derived from the ERS-1 triplet on Jutulstraumen Glacier. The bidirectional comparison shows that the mean distance is between 55 and 59m. Both GLLs are completely overlapped within 500m buffer distances.

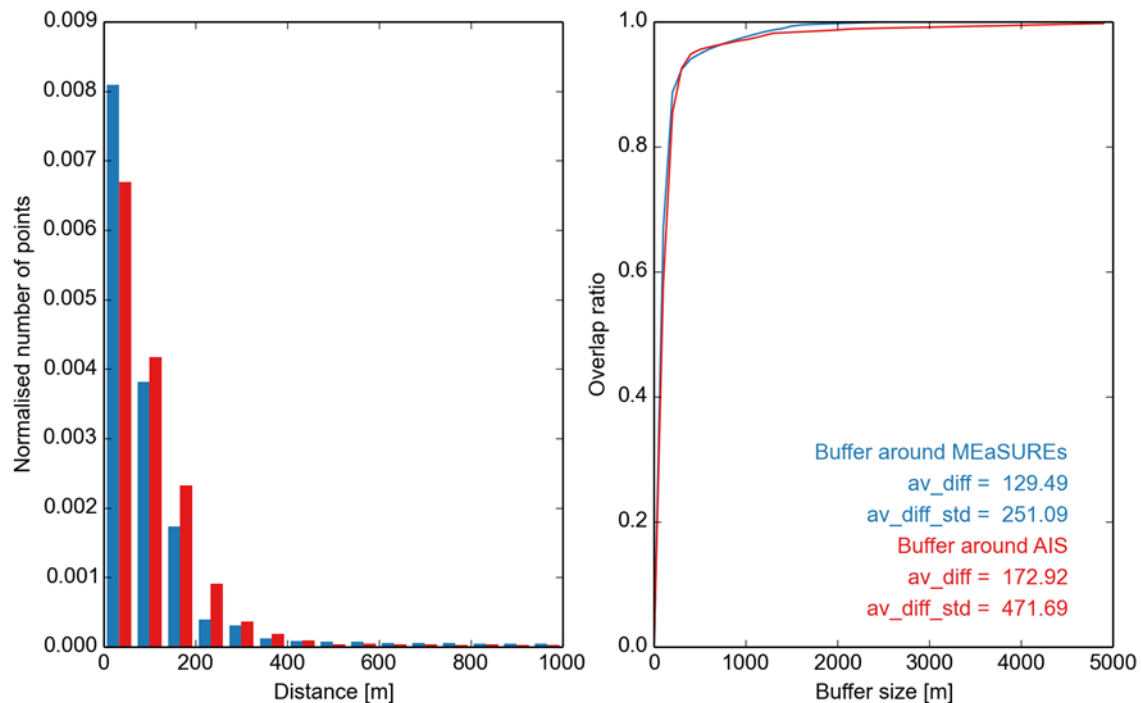


Figure 4.18: Same as Figure 4.17 but only GLL segments generated from Sentinel-1A data having counterparts in the two datasets are considered.

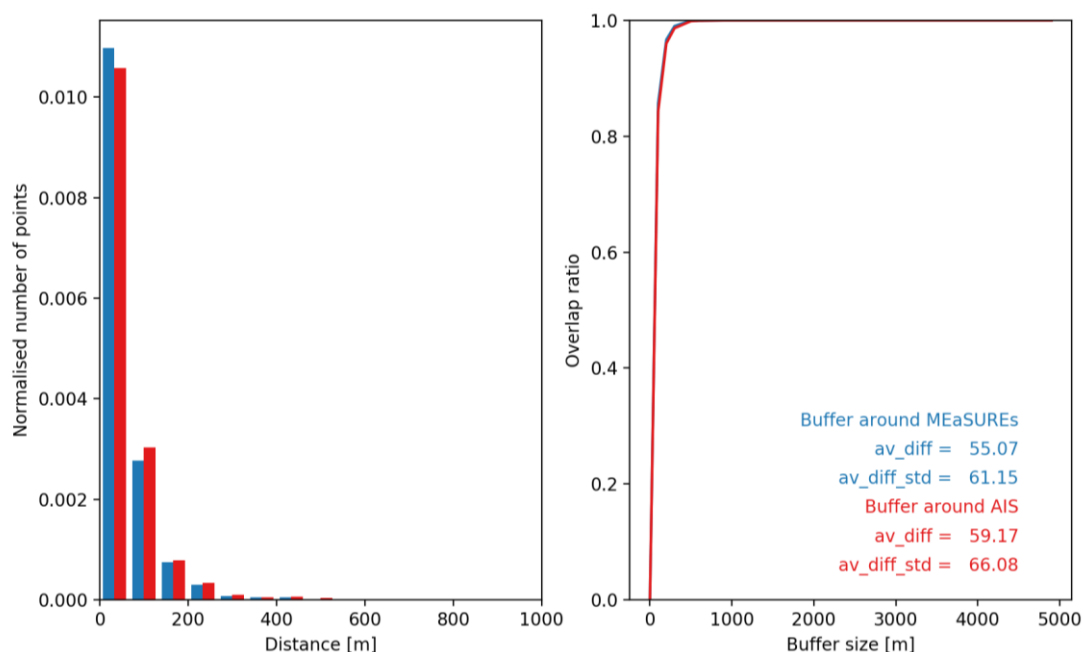


Figure 4.19: Same as Figure 4.18 (GLL has counterparts in both datasets) but for GLL segments generated from ERS-1.

Interpretation and explanation of validation outcome

Table 4-1 shows the mean distances of AIS_cci vs. ASAD, MOA and MEaSUREs for each investigated area as well as the overall average distances for each dataset (when all regions are included). In addition the average distances were also determined without PIG area since we think the time series contained in PIG MEaSUREs dataset biases the result and makes it worse than it actually is. One has to bear in mind that ocean tides were not considered or corrected in any of the used datasets and shifts in GLL within one tidal cycle can reach up to 10 km if either tides are strong or the subglacial topography is gentle.

The comparison of all validation datasets reveals that MEaSUREs and AIS_cci match best, in average with 576 m which is an extremely good agreement. It was expectable though that results which utilize the same methodology would provide similar results. ASAD is the next best fit with an average distance of 1.2 km, while MOA's average distance is 1.8 km. The histograms itself enable a more detailed understanding of which accuracy bands are represented in which dataset to which extent.

Regarding the comparison of the AIS_cci GLLs processed from the same Sentinel-1A and ERS-1 datasets the small values of the mean distances validate our products with respect to the MEaSUREs grounding line. Remaining differences can be caused by various error sources as e.g. differences in InSAR processing or fringe delineation. The differences are however in a range that is to be expected and can be accepted for an indirect measurement of the GLL. A more thorough validation of the actual spatial accuracy of the GLL can only be achieved by comparing in situ measurements of the GLL.

4.4 Recommendations for product improvement

There are currently no recommendations for product improvement.

4.5 Acknowledgements of data contributors for GLL validation

The following datasets were used for the present validation:

Haran, T., J. Bohlander, T. Scambos, T. Painter, and M. Fahnestock. 2005, updated 2013. MODIS Mosaic of Antarctica 2003-2004 (MOA2004) Image Map, Version 1. [Indicate subset used]. Boulder, Colorado USA. NSIDC: National Snow and Ice Data Center. doi: <http://dx.doi.org/10.7265/N5ZK5DM5>. [Accessed February 2016].

Bindschadler, R., H. Choi, and ASAD Collaborators. 2011. High-resolution Image-derived Grounding and Hydrostatic Lines for the Antarctic Ice Sheet. Boulder, Colorado, USA: National Snow and Ice Data Center. <http://dx.doi.org/10.7265/N56T0JK2>.

Rignot, E., J. Mouginot, and B. Scheuchl. 2011. Antarctic Grounding Line Mapping from Differential Satellite Radar Interferometry, *Geophysical Research Letters*. 38. L10504. <https://doi.org/10.1029/2011GL047109>

Rignot, E., J. Mouginot, and B. Scheuchl. 2016. *MEaSUREs Antarctic Grounding Line from Differential Satellite Radar Interferometry, Version 2*. [Indicate subset used]. Boulder, Colorado USA. NASA National Snow and Ice Data Center Distributed Active Archive Center. doi: <http://dx.doi.org/10.5067/IKBWW4RYHF1Q>. [Accessed March 2017].

Scheuchl, B., J. Mouginot, E. Rignot, M. Morlighem, and A. Khazendar (2016), Grounding line retreat of Pope, Smith, and Kohler Glaciers, West Antarctica, measured with Sentinel-1a radar interferometry data, *Geophys. Res. Lett.*, 43, 8572–8579, doi:10.1002/2016GL069287.

5 Gravimetric Mass Balance (GMB)

This chapter gives a complete report on the activities carried out to assess the quality of the GMB products. All assessments make use of the latest Climate Research Data Package (CRDP), published on 2017-12-08 via the AIS_cci GMB data portal (data1.geo.tu-dresden.de/ais_gmb). The data package relies on the GRACE monthly solution series ITSG-Grace2016 provided by TU Graz (Mayer-Gürr et al., 2016) and covers the period 2002-04 – 2016-08. The utilised GRACE series ITSG-Grace2016 includes spherical harmonic coefficients up to degree $l_{\max}=90$. Figure 5.1 shows the mass balance pattern (i.e. the linear trend) derived from the entire time series.

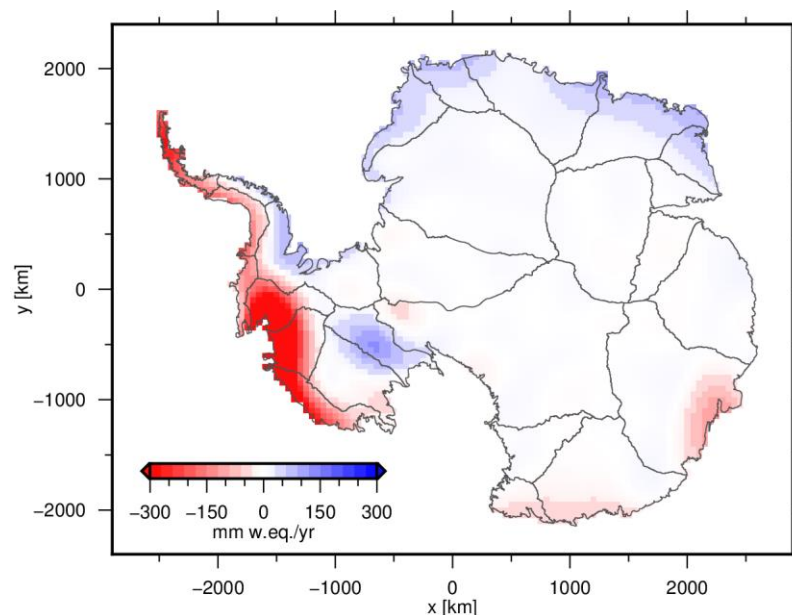


Figure 5.1: Spatial pattern of the linear trend in ice mass during the period 2002-04 – 2016-08.

5.1 Independent validation data

Requirements

An ideal validation data set would consist of an independent observation of the quantity to be validated, carried out by an alternative sensor, which is more precise and provides an identical spatial coverage at higher spatial resolution. In case of the GMB data set the validation data are required to provide observations of the change in ice mass with a temporal resolution of one month and a spatial resolution better than 50 km, while covering the entire AIS.

Unfortunately, no sensor except of GRACE is able to directly observe changes in mass with a comparable or even better spatial and temporal coverage. Hence, observations of alternative quantities related to mass changes have to be used after applying an appropriate conversion. For example, changes in the ice sheet's surface elevation can be converted into mass changes using an assumption of the density. The validation could also be based on the predictions of geophysical models. All these alternatives have the drawback of being dependent on additional assumptions and input data with their individual uncertainties.

Sources

Three major types of data sets are suitable for the GMB product validation. The following provides a brief description of the three data sets. An inter-comparison of results based on these types of data as well as on GRACE satellite gravimetry is given by Shepherd et al. (2012, SOM).

SEC

Surface elevation changes (SEC) of the AIS have been observed by different types of satellite altimetry missions, carrying laser (ICESat) or radar instruments (e.g. CryoSat-2). Satellite altimetry allows the precise mapping of SEC patterns, whereas radar altimetry provides the longest record with a monthly temporal sampling. Shepherd et al. (2012) compiled a SEC time series spanning the period from 1992 to 2010 from cross-calibrated observations of the radar satellites ERS-1, ERS-2 and ENVISAT. By including data from ESA's CryoSat-2 mission this time series can be continued until present.

Averaged over a certain drainage basin, volume changes need to be converted into mass changes in order to make them comparable to GMB products. Different approaches are used for this purpose. One approach makes use of a prescribed density model to discriminate between regions where fluctuations in elevation occur with the density of snow or ice (McMillan et al., 2014). Other studies make use of a firn compaction model (Ligtenberg et al., 2011) forced by a regional climate model (van Wessem et al., 2014) to correct SEC observations for fluctuations in the firn layer thickness.

SMB

Surface mass balance (SMB), defined as the difference between the mass gained by precipitation and the mass lost by sublimation and run-off, is one component of the ice sheets total mass balance (van den Broeke et al., 2011). Fluctuations in SMB can be predicted by regional climate models at high spatial (10-30 km) and temporal resolution (monthly) (Lenaerts et al., 2012), like the widely used model RACMO (van Wessem et al., 2014). For regions where the mass balance is dominated by changes in SMB, modelled cumulated SMB anomalies can be used for the inter-comparison with GMB time series.

IOM

The Input-output method (IOM) relies on the combination of mass input at the surface and mass loss through ice discharge into the ocean (van den Broeke et al., 2011). Information on the mass input are inferred from modelled fluctuations in SMB, while the mass loss component is derived from ice velocity and ice thickness information. For example, yearly ice velocity estimates can be derived from interferometric synthetic-aperture radar data. Ice thickness may be derived by radar echo sounding or by using satellite altimetry in combination with the hydrostatic equilibrium of the floating ice shelves (Rignot et al., 2011). After interpolating the slowly change discharge estimates, monthly mass balance estimates can be derived on the scale of individual drainage basins or for the entire AIS.

Assessment

Each of the three data sets introduced in the previous section comes with its individual strengths and weaknesses. For a comprehensive overview on the individual uncertainties cf. Shepherd et al. (2012) and references therein.

SEC observations may be biased by variations in the radar signal penetration into the firn layer. However, by far the largest uncertainties in SEC-based mass change time series arise from the conversion between volume and mass. Although the SEC patterns are provided at high spatial resolution, the polar gap prevents a complete coverage of the AIS.

Predicted fluctuations in SMB largely depend on the atmospheric forcing used as model input. Different global atmospheric reanalyses data sets used for SMB modelling yield significant differences in the model predictions. Consequently, these uncertainties are propagated to derived products, like firn densification models used in SEC processing.

IOM results are very sensitive to uncertainties in both components, i.e. modelled fluctuations in SMB and observed ice velocity and thickness (van den Broeke et al., 2011).

Selection

Considering the limited number of possible data sets suitable for the GMB product validation and the limitations of each of these data sets, a comprehensive validation needs to be based on the entire range of available sources. Unfortunately, only a few data sets are freely available. The following data sets could be used in the GMB quality assessment:

1. A SEC-based mass change time series for **different** drainage basins **and aggregations** derived from radar altimetry observations **were** provided by UL. The conversion from volume to mass was achieved using the density model described in Shepherd et al. (2012). This time series covers the period **1992 – 2017** and allows the inter-comparison with the corresponding time series from the GMB basin product (cf. PUG).
2. Monthly time series of basin-averaged cumulative SMB anomalies were derived from SMB predictions according to the regional climate model RACMO2.3 (van **Wessem et al., 2014**) with a spatial resolution of 27 km x 27 km. The entire time series covers the period between 1979 and **2016**.

5.2 Validation procedure

Since only two external data sets are available, the GMB quality assessment also comprises the inter-comparison of results based on different GRACE releases as well as results derived from synthetic data sets. In this way the performance of the selected algorithm, the quality of the utilised GRACE release and the overall quality of the final GMB products are proven. The following test and inter-comparisons were conducted.

- A. **GRACE releases:** The noise level of the monthly solutions from different GRACE releases is investigated. At this stage residuals w.r.t. a linear and seasonal modelled are analysed. The analysis is done in the spherical harmonic domain using the median degree amplitudes ($\sigma_l = \sqrt{\sum_{m=0}^l (c_{lm}^2 + s_{lm}^2)}$). In the spatial domain the median of all monthly residual maps is utilized to illustrate the noise level. For this purpose the monthly maps are smoothed using a Gaussian filter with a half-width of 400 km. Preliminary investigations revealed that the GRACE releases exhibiting the lowest noise level are provided by CSR (Release 05), UT Austin and by ITSG, TU Graz (ITSG-Grace2016). Hence, the inter-comparisons shown in the following section are limited to **146** monthly solutions between 2002 and 2016 common to these releases.

In addition, mass change time series for selected drainage basins and aggregations are compared. The design of the sensitivity kernels used for the regional integration depends on empirical GRACE error variance-covariances

inferred from the respective GRACE series in use. Hence, the sensitivity kernels would differ between the releases, which complicates a consistent inter-comparison. To ensure a minimum level of comparability, kernels for both releases are averaged and consistently applied to both series.

- B. **Synthetic data:** The utilized algorithm (cf. ATBD) is applied to a range of synthetic data sets with a priori known mass changes. By comparing the derived mass change estimates with the true mass changes, conclusion on the performance of the algorithm and induced signal leakage can be drawn. The synthetic data sets used are identical to those utilized for the Round Robin experiment (cf. annex to the ATBD).
- C. **SEC:** Mass change time series for **different drainage basins and aggregations** are compared w.r.t. their overall agreement and their individual mass balance estimates. The mass balance (i.e. the linear trend) is derived by fitting a linear, periodic (1 year, 1/2 year, 161 days) and quadratic model to the period common to both time series.
- D. **SMB:** Since the basin-averaged accumulated SMB anomaly time series solely represent the surface component of the total mass change, a direct comparison to the GMB basin product is not possible. Ice discharge shows only negligible seasonal variations and is clearly dominated by long-term signals. To ensure comparability, long-term signals (linear and quadratic) are removed from both the SMB and the GMB time series. The residual seasonal and inter-annual variations are mainly due to fluctuations in SMB. Correlations between both residual time series are used as indicators for the level of agreement.

5.3 Validation outcome

- A. **GRACE releases:** **Figure 5.4** shows the median degree amplitudes of the residuals derived from CSR RL05 96 and ITSG-Grace2016 series. For spherical harmonic degrees larger than 15 the degree amplitudes for ITSG-Grace2016 exhibit clearly less power, indicating a lower noise level. At higher degrees, which are dominated by errors, this difference becomes even larger. The same is true for the degree amplitudes calculated for spherical harmonic order $m=0...29$, only. Coefficients of these orders are of particular importance for studies in polar region.

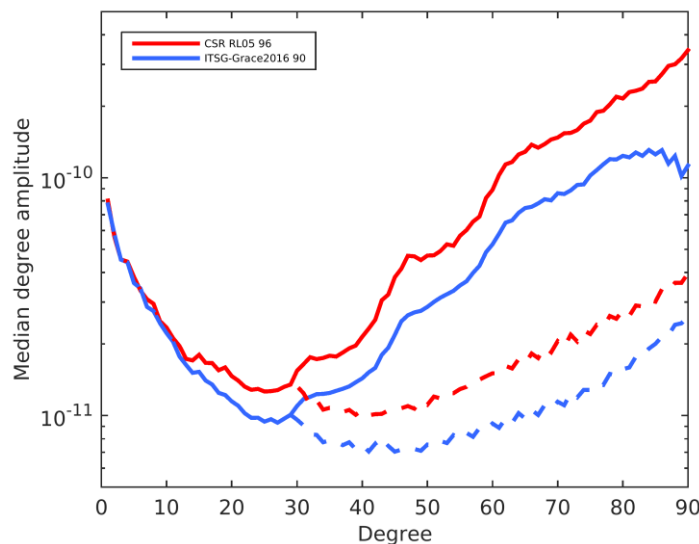


Figure 5.4: Median degree amplitudes of residual Stokes coefficients (solid lines). Dashed lines: Median degree amplitudes for order $m=0...29$.

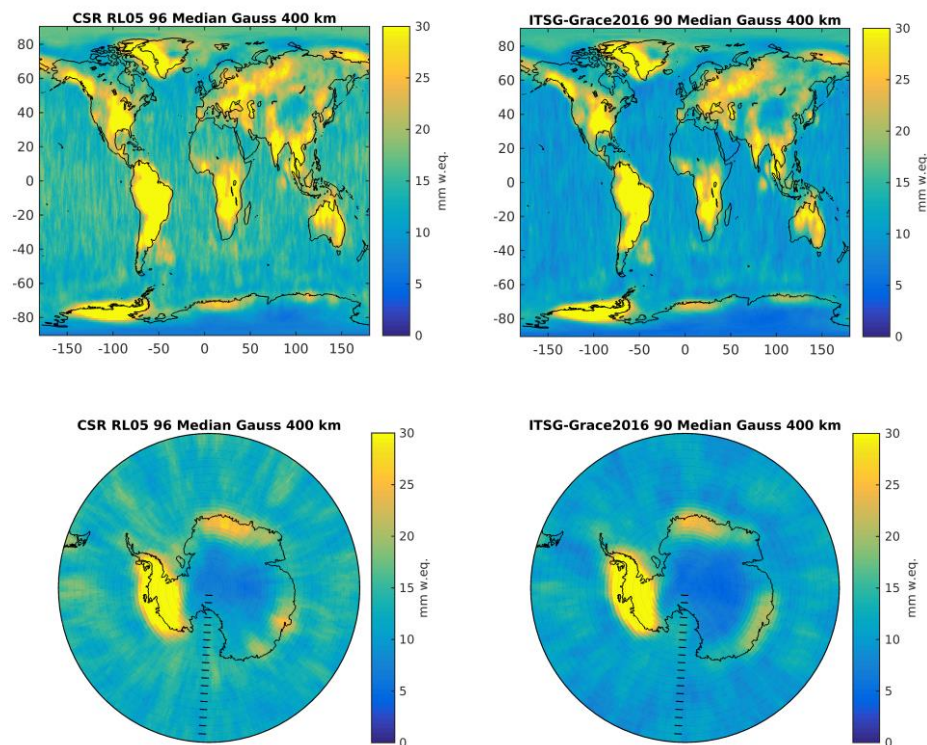


Figure 5.7: Global (top) and regional (bottom) maps of median residuals from CSR RL05 (left) and ITSG-Grace2016 (right) monthly GRACE series.

The spatial pattern of the median residuals is shown in Figure 5.7. Conclusions on the noise level can be derived by inspecting those regions apart from the prominent mass signals, e.g. the global oceans and the AIS interior. For the interior of the AIS the median residuals for ITSG-Grace2016 are smaller than for CSR RL05. Moreover, the region of low noise is larger and extended further towards the coast. Over the oceans the differences between both releases are even larger.

Less pronounced striping artefacts are visible in the ITSG-Grace2016 results. Results based on a weaker smoothing, e.g. a Gaussian filter with 200 km half-width, reveal even larger differences between the releases, which is in agreement with the median degree amplitudes shown in Figure 5.4.

The different noise levels of the releases is also revealed by the mass change time series for different aggregations of drainage basins shown in Figure 5.12. It is noteworthy that the long-term, inter-annual and seasonal signals of both series, depicted by the low-pass filtered time series, are comparable.

In summary, the demonstrated reduction in the noise level of the GMB products strongly suggests to utilise the GRACE series provided by ITSG.

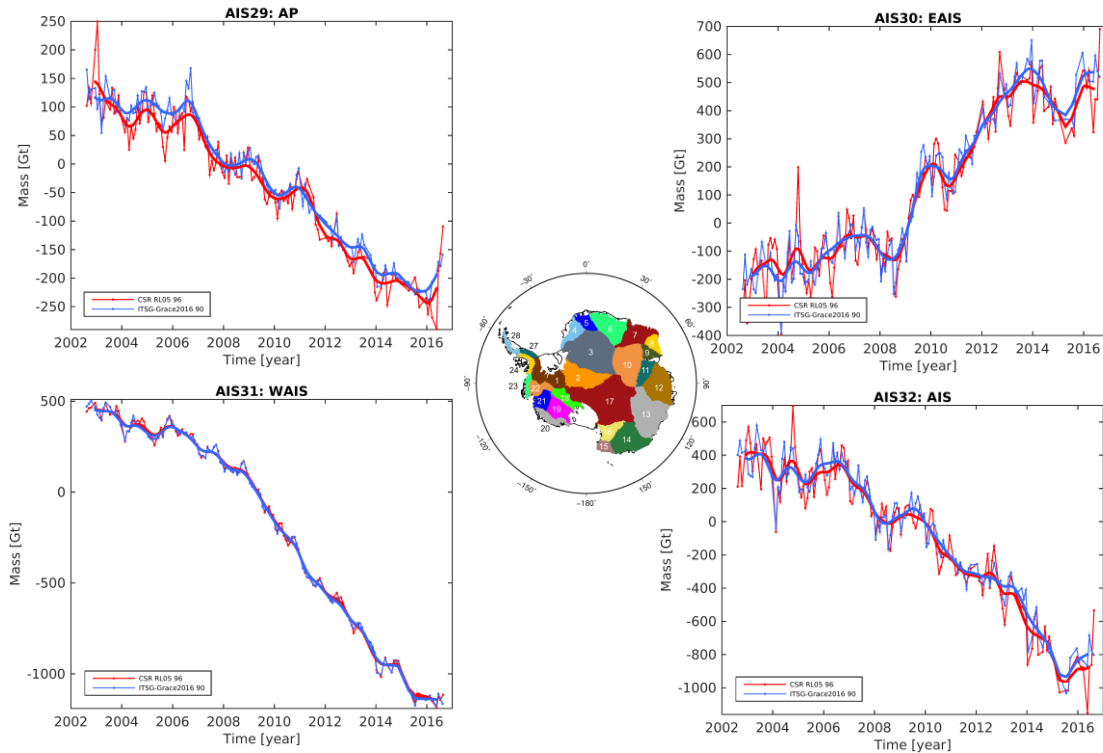


Figure 5.12: Mass change time series (thin lines) for the Antarctic Peninsula (AIS29: 24,27,28), East Antarctica (AIS30: 2:17), West Antarctica (AIS31: 1,18:23) and the entire AIS (AIS32). Bold lines: Low pass filtered time series. Red: CSR, blue: ITSG. Inset: Location and numbering of individual drainage basins.

B. Synthetic data: The overall performance of the applied algorithm was demonstrated in the Round Robin experiment. The entire set of results is annexed to the ATBD. Meanwhile, further modifications were adopted to the algorithm in order to find the optimal compromise between the minimisation of both GRACE error effects and signal leakage. The updated synthetic results are given in Figure 5.13. For example, the leakage error induced by the spatial pattern of the mean annual mass change of the AIS (data set number 7 – “AIS MB”) is 1 Gt only, corresponding to about 1% of the true mass change.

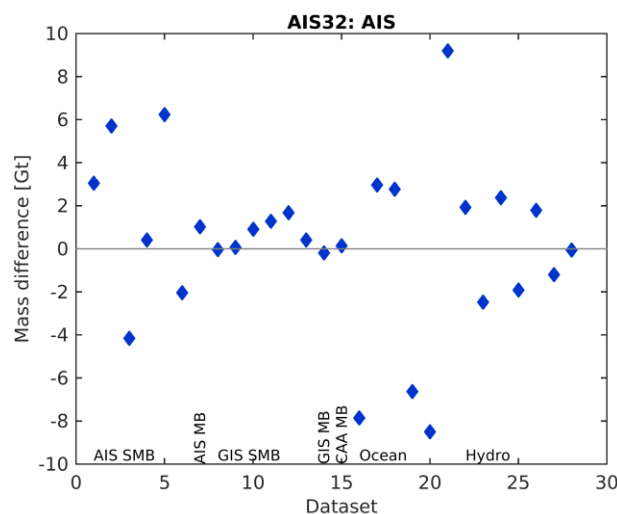


Figure 5.13: Differences between the mass changes derived from synthetic data sets and the corresponding synthetic 'true' mass change for the entire AIS (AIS32). The bottom row indicates the type of synthetic data set (cf. annex to ATBD).

- C. **SEC**: The comparison of the SEC- and GRACE-derived mass change time series for **East Antarctica (AIS30)** and **West Antarctica (AIS31)** is given in Figure 5.14. The mass loss dominating **West Antarctica**, mainly originating from the Amundsen Sea Sector, is revealed by both techniques. Larger differences are visible for **East Antarctica (AIS30)**, where the mass gain caused by two larger accumulation events in 2009 and 2011, is more pronounced in the GRACE mass change time series. The linear trend estimates over the common period given in Table 5-1 confirms the general better agreement for drainage basins exhibiting a negative mass balance (e.g. AIS20-AIS22) compared to basins with positive mass balance (e.g. AIS04-AIS08). However, considering the uncertainties inherent to each technique, as described in the CECR, none of the time series can be preferred over the other, making it difficult to perform a rigorous product validation.

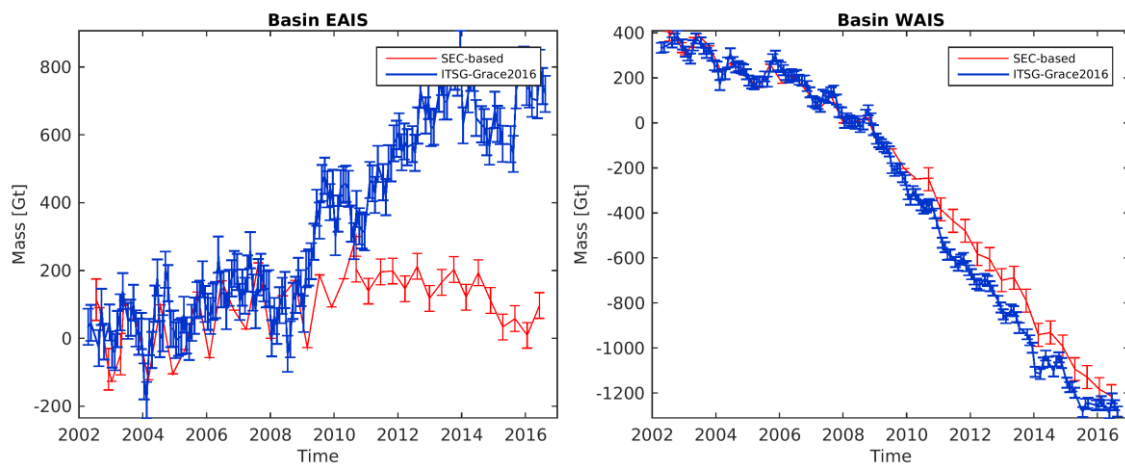


Figure 5.14: Mass change time series for the aggregation of basins AIS21 and AIS22 East Antarctica (left) and West Antarctica (right) (cf. inset Figure 5.12) derived from SEC and GRACE (ITSG-Grace2016) data.

Table 5-1: Linear trends for the period 2002-2016, derived from the mass change time series based on SEC and GRACE. Uncertainties are formal errors from the least squares adjustment.

Basin ID	Linear trend GRACE [Gt/yr]	Linear trend SEC [Gt/yr]	Basin ID	Linear trend GRACE [Gt/yr]	Linear trend SEC [Gt/yr]
AIS01	5.05 ± 0.37	4.48 ± 0.15	AIS14	-7.58 ± 0.48	-5.58 ± 0.30
AIS02	2.04 ± 0.20	1.55 ± 0.13	AIS15	-3.73 ± 0.16	-3.68 ± 0.20
AIS03	14.77 ± 0.34	6.87 ± 0.36	AIS16	0.76 ± 0.11	0.52 ± 0.09
AIS04	10.12 ± 0.25	3.48 ± 0.24	AIS17	4.31 ± 0.40	5.24 ± 0.26
AIS05	7.46 ± 0.23	3.45 ± 0.16	AIS18	14.77 ± 0.13	12.94 ± 0.37
AIS06	16.93 ± 0.48	6.37 ± 0.37	AIS19	0.73 ± 0.17	-0.31 ± 0.21
AIS07	17.21 ± 0.48	5.28 ± 0.32	AIS20	-35.88 ± 0.42	-24.65 ± 0.37
AIS08	6.55 ± 0.22	2.98 ± 0.10	AIS21	-54.95 ± 0.34	-62.15 ± 0.26
AIS09	1.25 ± 0.12	1.06 ± 0.11	AIS22	-50.80 ± 0.37	-44.71 ± 0.38
AIS10	3.21 ± 0.19	-0.31 ± 0.23	AIS23	-9.45 ± 0.17	-5.45 ± 0.17
AIS11	-0.62 ± 0.13	-0.66 ± 0.09	AIS30	62.73 ± 2.01	9.74 ± 2.10
AIS12	3.41 ± 0.39	-2.56 ± 0.28	AIS31	-130.54 ± 1.54	-119.76 ± 1.45

AIS13	-13.35 ± 0.60	-14.52 ± 0.64			
--------------	----------------------	----------------------	--	--	--

D. **SMB:** Figure 5.15 compares residual mass change time series from RACMO2.3 and GRACE for selected drainage basins and aggregations. The differences in the high-frequent signal components, mainly caused by noise in the GRACE series, hampers a direct comparison, in particular for basins with small fluctuations in SMB (e.g. AIS08, AIS16). Low-pass filtered time series are more suitable to study the agreement between both data sets. Time series for the larger aggregations (AIS29-AIS32) exhibit comparable seasonal and inter-annual variation. Pronounced signals, like caused by the 2009 and 2011 accumulation events in Dronning Maud Land, are equally revealed by both series (cf. AIS30).

The correlation coefficients listed in Table 5-2 reveal the general good agreement between the results from GRACE and RACMO2.3. By nature, the majority of basins reveal an increased level of agreement for the low-pass filtered results. Only for a few smaller basins, exhibiting low variations in SMB, no correlation is found between the two time series (cf. AIS27).

Table 5-2: Correlation coefficients between the time series of residual mass changes from RACMO2.3 and GRACE.

Basin ID	Correlation original time series	Correlation low-pass filtered time series	Basin ID	Correlation original time series	Correlation low-pass filtered time series
AIS01	0.840	0.925	AIS16	0.499	0.778
AIS02	0.281	0.591	AIS17	0.531	0.818
AIS03	0.637	0.907	AIS18	0.604	0.753
AIS04	0.851	0.982	AIS19	0.695	0.875
AIS05	0.792	0.953	AIS20	0.945	0.983
AIS06	0.910	0.989	AIS21	0.815	0.875
AIS07	0.849	0.980	AIS22	0.848	0.933
AIS08	0.248	0.533	AIS23	0.762	0.786
AIS09	0.330	0.629	AIS24	0.860	0.946
AIS10	0.400	0.760	AIS27	0.066	0.245
AIS11	0.373	0.664	AIS28	0.568	0.798
AIS12	0.784	0.879	AIS29	0.740	0.880
AIS13	0.802	0.922	AIS30	0.749	0.926
AIS14	0.823	0.962	AIS31	0.939	0.973
AIS15	0.308	0.720	AIS32	0.673	0.814

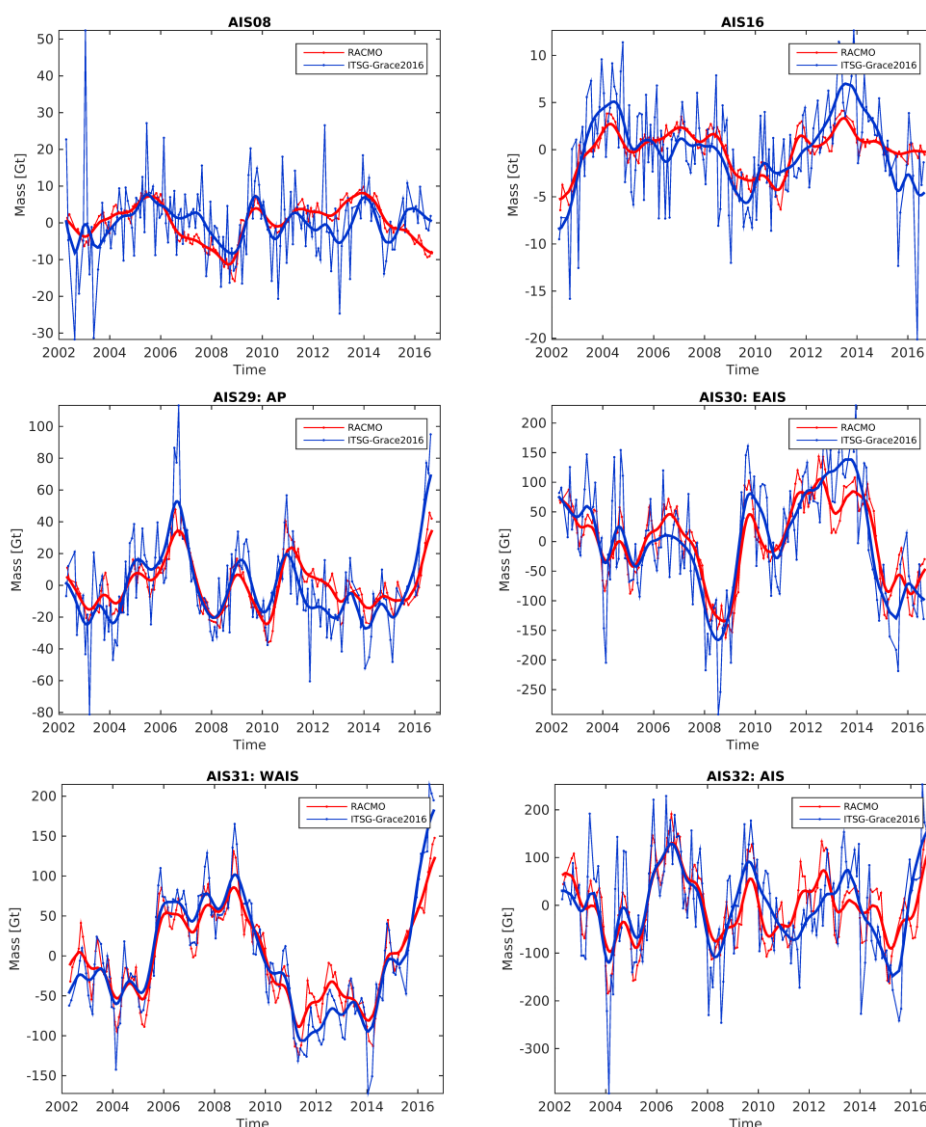


Figure 5.15: Residual mass change time series from RACMO2.3 and GRACE (thin lines) for selected drainage basins and aggregations. Red: CSRRACMO, blue: ITSG. Linear and quadratic signal components are removed. Bold lines: Low-pass filtered time series.

5.4 Recommendations for product improvement

Future algorithm improvements will focus on the incorporation of more realistic GRACE error information, e.g. by using actual GRACE variance/co-variances matrices instead of empirical estimates. Moreover, to further improve the GMB product validation, it will be necessary to extend the existing archive of external data sets, e.g. by means of SEC-based time series for the Antarctic Peninsula.

5.5 Acknowledgements of data contributors for GMB validation

We acknowledge the support by UL and the Institute for Marine and Atmospheric Research Utrecht (IMAU) who provided SEC mass change time series and fluctuations in SMB predicted by RACMO2.3, respectively.

6 References

- British Antarctic Survey (2005). Antarctic factsheet geographical statistics. British Antarctic Survey, Natural Environment Research Council.
https://www.bas.ac.uk/wp-content/uploads/2015/05/factsheet_geostats_print.pdf (last access April 2016)
- Bindschadler, R., H. Choi, A. Wichlacz, R. Bingham, J. Bohlander, K. Brunt, H. Corr, R. Drews, H. Fricker, M. Hall, R. Hindmarsh, J. Kohler, L. Padman, W. Rack, G. Rotschky, S. Urbini, P. Vornberger, and N. Young. 2011. Getting around Antarctica: New High-Resolution Mappings of the Grounded and Freely-Floating Boundaries of the Antarctic Ice Sheet Created for the International Polar Year. *The Cryosphere*, 5, 569-588. doi:10.5194/tc-5-569-2011.
- van den Broeke, M., Bamber, J., Lenaerts, J., & Rignot, E. (2011). Ice Sheets and Sea Level: Thinking Outside the Box. *Surv. Geophys.*, 32(4), 495–505.
- Burton-Johnson, A., Black, M., Fretwell, P. T., and Kaluza-Gilbert, J.: An automated methodology for differentiating rock from snow, clouds and sea in Antarctica from Landsat 8 imagery: a new rock outcrop map and area estimation for the entire Antarctic continent, *The Cryosphere*, 10, 1665-1677, <https://doi.org/10.5194/tc-10-1665-2016>, 2016.
- Heo, J., Kim, J.H. and Kim, J.W., 2009. A new methodology for measuring coastline recession using buffering and non-linear least squares estimation. *International Journal of Geographical Information Science*, 23(9), pp.1165-1177.
- Jeong, S., Jung, J., Kim, S., Hong, S., Sohn, H.G. and Heo, J., 2014. Buffering-based approach to fluctuation analysis of glacier calving fronts using LANDSAT-7 ETM+, with a case study of Jakobshavn Isbræ. *Computers & Geosciences*, 64, pp.115-125.
- Lenaerts, J. T. M., van den Broeke, M. R., van de Berg, W. J., van Meijgaard, E., & Kuipers Munneke, P. (2012). A new, high-resolution surface mass balance map of Antarctica (1979-2010) based on regional atmospheric climate modeling. *Geophys. Res. Lett.*, 39(4), L04501.
- Ligtenberg, S. R. M., Helsen, M. M., & van den Broeke, M. R. (2011). An improved semi-empirical model for the densification of Antarctic firn. *The Cryosphere*, 5(4), 809–819.
- Mayer-Gürr, T., Behzadpour, S., Ellmer, M., Kvas, A., Klinger, B., & Zehentner, N. (2016). ITSG-Grace2016 – Monthly and Daily Gravity Field Solutions from GRACE. GFZ Data Services, doi:10.5880/icgem.2016.007
- McMillan, M., Shepherd, A., Sundal, A., Briggs, K., Muir, A., Ridout, A., Hogg, A., & Wingham, D. (2014). Increased ice losses from Antarctica detected by CryoSat-2. *Geophys. Res. Lett.*, 41(11), 3899–3905.
- Rignot, E., Velicogna, I., van den Broeke, M. R., Monaghan, A., & Lenaerts, J. (2011). Acceleration of the contribution of the Greenland and Antarctic ice sheets to sea level rise. *Geophys. Res. Lett.*, 38(5), L05503.
- Rignot, E., J. Mouginot, and B. Scheuchl. 2011. Antarctic Grounding Line Mapping from Differential Satellite Radar Interferometry, *Geophysical Research Letters*. 38. L10504.
<http://dx.doi.org/10.1029/2011GL047109>
- Rignot, E., J. Mouginot, and B. Scheuchl. 2017. MEaSURES InSAR-Based Antarctica Ice Velocity Map, Version 2. Boulder, Colorado USA. NASA National Snow and Ice Data Center Distributed Archive Center. doi: <http://dx.doi.org/10.5067/D7GK8F5J8M8R>. [3 May 2017].
- Scambos, T., T. Haran, M. Fahnestock, T. Painter, and J. Bohlander. 2007. MODIS-based Mosaic of Antarctica (MOA) Data Sets: Continent-wide Surface Morphology and Snow Grain Size. *Remote Sensing of Environment* 111(2): 242-257. <http://dx.doi.org/10.1016/j.rse.2006.12.020>.
- Shepherd, A., Ivins, E. R., A. G., Barletta, V. R., Bentley, M. J., Bettadpur, S., Briggs, K. H., Bromwich, D. H., Forsberg, R., Galin, N., Horwath, M., Jacobs, S., Joughin, I., King, M. A., Lenaerts, J. T. M., Li, J., Ligtenberg, S. R. M., Luckman, A., Luthcke, S. B., McMillan, M., Meister, R., Milne, G., Mouginot, J., Muir, A., Nicolas, J. P., Paden, J., Payne, A. J., Pritchard, H., Rignot, E., Rott, H., Sorensen, L. S., Scambos, T. A., Scheuchl, B., Schrama, E. J. O., Smith, B., Sundal, A. V., van Angelen, J. H., van de Berg, W. J., van den Broeke, M. R., Vaughan, D. G., Velicogna, I., Wahr, J., Whitehouse, P. L., Wingham, D. J., Yi, D., Young, D., & Zwally, H. J. (2012). A Reconciled Estimate of Ice-Sheet Mass Balance. *Science*, 338(6111), 1183–1189.
- Van Wessem, J. M., Reijmer, C. H., Morlighem, M., Mouginot, J., Rignot, E., Medley, B., Joughin, I., Wouters, B., Depoorter, M. A., Bamber, J. L., Lenaerts, J. T. M., De Van Berg, W. J., Van Den Broeke, M. R., & Van Meijgaard, E. (2014). Improved representation of East Antarctic surface mass balance in a regional atmospheric climate model. *J. Glac.*, 60(222), 761–770. doi:10.3189/2014JoG14J051